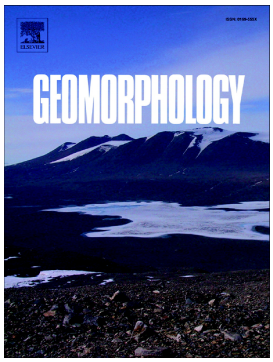

Reconstructing paleolakes in Nepenthes Mensae, Mars, using the distribution of putative deltas, coastal-like features, and terrestrial analogs

Ángel García-Arnay, Francisco Gutiérrez

PII: S0169-555X(20)30101-X

DOI: https://doi.org/10.1016/j.geomorph.2020.107129

Reference: GEOMOR 107129

To appear in: *Geomorphology*

Received date: 4 December 2019

Revised date: 6 February 2020

Accepted date: 27 February 2020

Please cite this article as: Á. García-Arnay and F. Gutiérrez, Reconstructing paleolakes in Nepenthes Mensae, Mars, using the distribution of putative deltas, coastal-like features, and terrestrial analogs, *Geomorphology*(2020), https://doi.org/10.1016/j.geomorph.2020.107129

Reconstructing paleolakes in Nepenthes Mensae, Mars, using the distribution of putative deltas, coastal-like features, and terrestrial analogs

Ángel García-Arnay[(a)*], Francisco Gutiérrez[(a)]

[a] Departamento de Ciencias de la Tierra, Universidad de Zaragoza, 50009 Zaragoza, Spain

* Corresponding author e-mail address: arnay@unizar.es

Abstract

Nepenthes Mensae is an equatorial region situated north of the Martian dichotomy, northwest of Gale crater. It is characterized by a NW-SE-oriented belt of interconnected depressions, Late Noachian to Early Hesperian in age, with knobby terrains with residual relief. The highlands south of Nepenthes Mensae, Middle Noachian in age, correspond to the Licus Vallis region, which is dissected by drainage networks with valley mouths located along the dichotomy boundary scarp. This work presents a detailed geomorphological analysis of ten fan-shaped and fifty-four coastal-like benches identified in Nepenthes Mensae. The combination of detailed mapping, morphological and morphometric analyses, spatial-altitudinal distribution relationships, crater counting, spectral analysis, and comparison with terrestrial analogs suggest that (1) the fan-shaped and coastal-like benches are likely putative Gilbert-type deltas and paleoshore platforms, respectively, and (2) these features may be attributable to paleoshorelines developed along the margins of an ancient inner sea or interconnected

paleolakes. These findings reveal the important morphogenetic role that liquid water played in the evolution of Nepenthes Mensae and Licus Vallis regions during the Late Noachian-Early Hesperian transition, and contribute to contextualize the continuous findings on the environmental and climatic conditions of the nearby Gale crater during such time period.

Keywords: Mars; Hydrology; Fan-shaped deposit; Paleo-water level; Desiccated lake.

1. Introduction

Multiple geomorphological and geochemical lines of evidence indicate that liquid water has played an instrumental role during the early evolutionary stages of Mars (e.g., Baker, 2001; Bibring et al., 2006), as well as during relatively short periods in recent times (e.g., Malin and Edgett, 2000). Numerous valley networks carved into the Noachian highlands may be the result of past runoff erosion (e.g., Irwin et al., 2005), and/or a combination of runoff and groundwater sapping erosional processes (Malin and Carr, 1999; Harrison and Grimm, 2005). Large outflow channels developed during the Hesperian and Amazonian periods are attributed to the catastrophic release of large amounts of groundwater (Andrews- Hanna and Phillips, 2007). Fan-shaped deposits associated with the mouth of stream networks debouching at various types of depressions have been widely reported on Mars (e.g., Kleinhans, 2005; Di Achille and Hynek, 2010a). Such features, which show morphologic characteristics analogous to those of deltas on Earth, occur in spatially restricted closed basins such as impact craters (e.g., Goudge et al., 2015), some of them with outlet valleys, and in large basins, commonly where valley networks reach the edge of depressions or the upland-lowland

boundary (e.g., Fassett and Head, 2008). Some of the best-known delta-like features on Mars are probably the Jezero and the Eberswalde deltas, which show multiple lobes with clearly visible distributary channels with a meandering pattern (Wood, 2006; Pondrelli et al., 2008; Schon, 2012). The presence of deltas supports the existence in the past of long-standing liquid water bodies in paleolakes and an ancient ocean developed in the Martian lowlands (e.g., Head et al., 1999; Carr and Head, 2003; Di Achille and Hynek, 2010b; Fawdon et al., 2018). Laterally continuous benches with consistent elevation along the margins of the Lowlands and depressions have been interpreted as possible erosional and/or aggradational coastal landforms that record paleoshorelines (e.g., Parker et al, 1993; Ghatan and Zimbelman, 2006).

Irwin et al. (2005) reported fan-shaped deposits and ascribed them to a Gilbert-type delta in Nepenthes Mensae, which was also analyzed by de Pablo and Pacifici (2008). The rest of fan-shaped deposits documented in this work (i.e., 9 out of 10) were presented, for the first time, by García-Arnay (2016) and García-Arnay et al. (2018b, c). Recently, Rivera-Hernández and Palucis (2019) have also documented some of these landforms that can be used as possible paleoshoreline markers in the equatorial region of Nepenthes Mensae (e.g., de Pablo and Pacifici, 2008; de Pablo and Pacifici, 2009; Valenciano et al., 2009; García-Arnay, 2016; García-Arnay et al., 2018a). These features may record the past existence of a long-lived body of liquid water related to the putative Martian ocean.

In this work, we present a geomorphological analysis of Nepenthes Mensae, largely based on detailed geomorphic mapping. It explores features attributable to deltas and shore platforms related to an ancient inner sea or a system of paleolakes, and reinforces

this interpretation using possible terrestrial analogs. These putative paleoshore markers are characterized by analyzing their morphometric features and their surface composition, and estimating their numerical age. Paleowater-level elevations derived from the putative deltas and shore platforms are used to reconstruct the paleogeography of the inferred paleolakes (e.g., extent, depth, volume).

2. Study area

The study area is located in an equatorial region of the eastern hemisphere of Mars, astride two contrasting geomorphic domains divided by the Martian dichotomy boundary scarp: Nepenthes Mensae and Licus Vallis region (Fig. 1). Nepenthes Mensae (centered at 2°N, 124°E) is situated north of the dichotomy (upland-lowland boundary), east of Isidis Planitia, and northwest Gale crater. This region is characterized by a belt of interconnected NW-SE-trending depressions (de Pablo and Pacifici, 2009) with knobby terrains of residual relief (mesas and knobs) related to the erosion of the Martian highlands along the dichotomy (Caprarelli, 2015). The dichotomy displays steep slopes ~2 km in local relief. Nepenthes Mensae was mapped as Hesperian-Noachian transition unit (HNt) and interpreted as volcanic deposits, impact breccias, and sediments of Noachian in age with aprons formed by Hesperian mass-wasted deposits, according to the most recent global geological map of Mars (Tanaka et al., 2014). The highlands south of Nepenthes Mensae correspond to the Licus Vallis region (centered at 4°S, 125°E), an ancient fluvial valley (e.g., Irwin and Howard, 2002) located in the northeastern part of Mare Tyrrhenum quadrangle. It was mapped as middle Noachian highland unit (mNh), which is interpreted as “moderately to heavily degraded” “undifferentiated impact, volcanic, fluvial and basin materials” (Tanaka et al., 2014).

The heavily cratered terrains of Licus Vallis region are dissected by V-shaped valley networks related to fluvial erosion, whose mouths are located along the dichotomy. Sapping erosion may also have contributed to the headward expansion of valleys, as supported by the existence of theater-shaped valley heads (Vaquero and Hernández, 2010). Licus Vallis shows a very low drainage density and an apparently poorly-developed watershed, as suggested by its convex hypsometric curve (García-Arnay et al., 2018c). The knickpoints, slope breaks and paired terraces recognized within the valleys support base-level changes that could

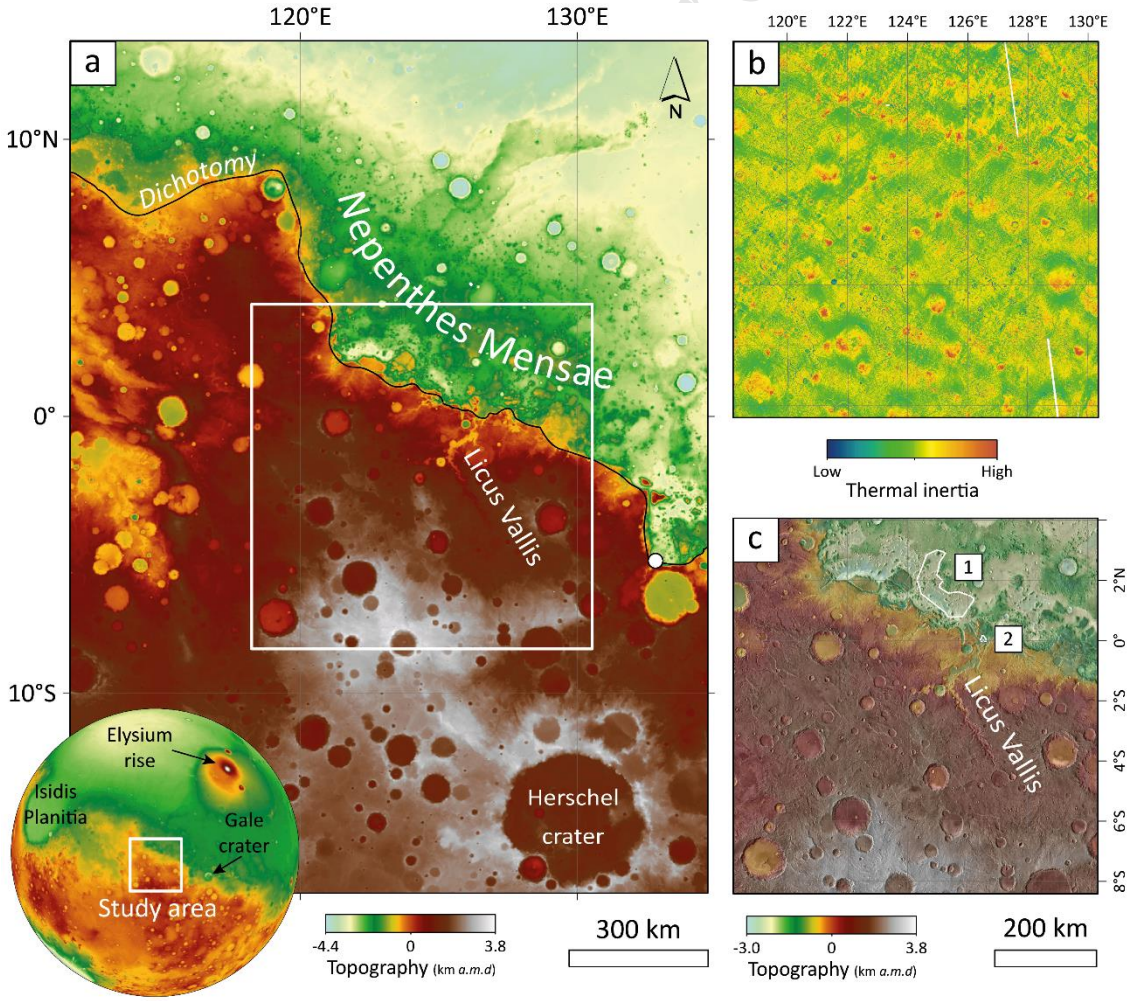

Fig. 1. (a) Colorized elevation model (kilometers above Martian datum, a.m.d.) derived from MOLA, with the study area framed by the white box. The small white circle east of study area marks the position of the fan-delta whose surface composition was inferred by CRISM spectral analysis. (b) Qualitative thermal inertia mosaic of the study area derived from THEMIS. (c) Colorized elevation model of the study area derived from HRSC-MOLA blended data over a mosaic of THEMIS-IR day images. White-lined polygons represent the crater-counting areas delineated for dating the depressions and the largest delta (labelled as 1 and 2, respectively).

be related to water-level variations in the mouth area and/or vertical tectonic movements (Goudge and Fassett, 2018). The transition between both geomorphic domains is dominated by the presence of morpho-structural lineaments (Martín-González et al., 2007) that may have controlled the erosion of the highlands as well as the drainage pattern along the dichotomy.

3. Data and methods

Imagery as well as topographic and spectral data were used to characterize the geomorphology and surface composition of the analyzed region. Visible imagery included panchromatic images acquired by the High Resolution Stereo Camera (HRSC, 12.5 m/pixel) (Neukum et al., 2004) on board the ESA's Mars Express, as well as by the Context Camera (CTX, 5-6 m/pixel) (Malin et al., 2007; Dickson et al., 2018) and the High Resolution Imaging Science Experiment (HiRISE, ~25-50 cm/pixel) (McEwen et al., 2007), both instruments on board the NASA's Mars Reconnaissance Orbiter. Additional information was extracted from the qualitative thermal inertia image mosaic

derived from nighttime infrared images obtained by the Thermal Emission Imaging System (THEMIS, 100 m/pixel) (Christensen et al., 2004, 2013) on board NASA's Mars Odyssey. Thermal inertia (TI) permits the differentiation of surface materials based on their thermophysical properties. In this work, TI data helped in identifying and mapping drainage networks because unconsolidated sediments such as eolian deposits, characterized by lower apparent TI, mainly occur in low-lying areas such as fluvial valleys.

Topographic data were extracted from Digital Elevation Models (DEMs) derived from laser altimeter point shots acquired by the Mars Orbiter Laser Altimeter (MOLA, 463 m in resolution) (Zuber et al, 1992), on board NASA's Mars Global Surveyor, as well as images from the HRSC instrument (50-75 m/pixel). In order to cover areas where no HRSC data were available, we used a blend of DEM data derived from MOLA and HRSC (Fergason et al., 2018, ~200 m/pixel). The spatial resolution of the HRSC-derived topography, that covers almost all the study area, is appropriate for analyzing the landforms of interest for this work. Imagery and topographic data were integrated into a Geographic Information System (ArcGIS 10.5.1, ESRI) for mapping and carrying out multiple morphological and morphometric analyses. Spatial data were projected into the same geographic coordinate system with sinusoidal projection and central meridian located in the center of the study area (125ºE).

Surface composition was inferred from hyperspectral data acquired by the Compact Reconnaissance Imaging Spectrometer for Mars (CRISM, ~18 m/pixel) aboard NASA's Mars Reconnaissance Orbiter, a visible-infrared imaging spectrometer sensitive to light from 0.362 to 3.92 μm (Murchie et al., 2007). Spectral data were retrieved from the

PDS Geosciences Node Mars Orbital Data Explorer (ODE) (available at: https://ode.rsl.wustl.edu/mars/) in corrected I/F (radiance/solar irradiance) using Targeted Empirical Record (TER) and Map-projected Targeted Reduced Data Record (MTRDR) products. We carried out the spectral analysis using the corrected I/F to obtain spectral diagrams, and the refined spectral summary parameters to derive spectral parameter maps (Viviano-Beck et al., 2014). Spectral data were processed using the CRISM Analysis Toolkit (CAT, version 7.3.1), an IDL/ENVI-based software system developed by the CRISM Science Team (Morgan et al., 2014). Due to its paleoenvironmental interest, clay-bearing surfaces were highlighted in a spectral parameter map obtained by the PHY product (D2300 (red), D2200 (green), BD1900r2 (blue)) for the projected CRISM observation FRT000064CE (~18 m/pixel, and ~10 km across) (Fig. 4b below) following the procedure described by Viviano-Beck et al. (2014). The values displayed for each RGB channel were adjusted applying stretch limits to highlight the clay-bearing materials. The I/F spectrum was extracted from the unprojected CRISM cube and averaged from a Region of Interest (ROI) drawn for the compositional unit. This average spectrum (s1) was ratioed to an average spectrum from a ROI of spectrally unremarkable terrains (s2) from the CRISM scene to minimize atmospheric contributions and instrument artifacts. The ratioed I/F spectrum (i.e., s1/s2) was compared with the CRISM spectral library (available at: http://crismtypespectra.rsl.wustl.edu/) (Viviano-Beck et al., 2015). The choice of this CRISM scene was determined by (1) the absence of TER products for fan-shaped deposits within the study area, and (2) the scene corresponds to a previously interpreted fan delta located close to the study area.

In order to identify equipotential surfaces corresponding to paleolevels of possible long-standing liquid-water bodies, we extracted the elevation values (expressed in meters above Martian datum, a.m.d.) from the mapped putative deltaic and coastal-like landforms (e.g., Irwin and Zimbelman, 2012). In the case of putative deltas, we considered the slope break at the junction between the delta plain and the delta front, which was interpreted as the mean highstand (e.g., Di Achille, and Hynek, 2010b). In spite of the difficulties to infer the water level from the elevation of shore platforms on Earth (e.g., Trenhaile, 1987; Sunamura, 1992), we decided to consider the inner edge, also called the "shoreline angle" (e.g., Figueiredo et al., 2014; Zazo et al., 2013; Hearty et al., 2007) (Fig. 2). The spatial-altitudinal distribution of the putative deltas and benches (Fig. 8) permitted us to constrain their elevation range, and reconstruct the distribution of ancient liquid-water bodies (Fig. 9). The approximate volume of the largest mass of liquid water was measured using the ArcGIS tool "Polygon volume". It calculates the volume resulting from the intersection between the lake bottom derived from a TIN model and a horizontal surface defined by the mean elevation estimated for the water level. The maximum depth was estimated by the difference between the mean elevation of the water level and the elevation of the deepest bathymetry point, which was calculated using the ArcGIS tool "Zonal Statistics as Table", while the mean depth is given by the difference between the mean water level elevation and the average elevation of the bathymetry of the depression. In this research, we assumed that (1) the present regional topography is similar to the one that existed during the development of the analyzed landforms, and (2) the landforms formed when the Martian hydrosphere was persistent and a long-standing body of liquid water was present in the region (e.g., Di Achille and Hynek, 2010b). The stream network and watershed boundaries were mapped using the toolset "Hydrology" of ArcGIS. The drainage network generated

automatically, which included numerous artifacts, was improved manually using imagery and TI data. Watershed boundaries were delineated considering the local base levels defined by each putative delta at the mouth of drainage basins.

The mapping of some putative deltas was challenging due to their spatially variable preservation conditions and geomorphic setting. The proximal edges of the deltas were delineated where the ancient flow debouching from the fluvial valley became unconfined (Fig. 2). The areas estimated for some deltas should be considered as minimum values due to surface reduction related to erosional processes (e.g., landsliding). The delta-shape index, or elongation of the delta, is a dimensionless morphometric parameter defined by the expression $S_d = W_d/2L_d$, where L_d is the delta length given by the maximum distance parallel to the paleoflow direction and W_d is the delta width, defined as the maximum distance across the foot of the delta front and perpendicular to W_d. S_d values of 1 correspond to semicircular deltas, while $S_d > 1$ and $S_d < 1$ indicate oblate and prolate deltas with long axes perpendicular or parallel to the paleoflow direction, respectively. These definitions were adapted for this work from Caldwell and Edmonds (2014) (see Fig. 2). We also estimated the mean slope for the deltaic plains and fronts, as well as several morphological attributes as defined by Di Achille and Hynek, (2010a) in order to characterize qualitatively: (1) the type of drainage network, distinguishing between poorly-developed stream networks (Lw) and steep canyons (C); (2) the morphology of the delta front, differentiating between steep simple fronts (M1) and stepped fronts with benches or slope breaks (M2); (3) evidence of avulsion (multi-lobate deltas); and (4) visible layering (see Table 1).

Surface dating was carried out using the crater size-frequency distribution (CSFD) method (e.g., Neukum et al., 2001, Hartmann and Neukum, 2001) in order to estimate the age of the morphogenetic surface and resurfacing events. Impact craters and crater-counting areas (Fig. 1c) were mapped using the CraterTools toolset for ArcGIS (Kneissl et al., 2011). Crater size-frequency diagrams were generated using CraterStats2 software (Michael and Neukum, 2010), and age estimates (Fig. 6) were derived using the production and chronology functions defined by Hartmann (2005). The clustering of the crater population and the confidence level of its adjustment was determined by the randomness analysis (Michael et al., 2012).

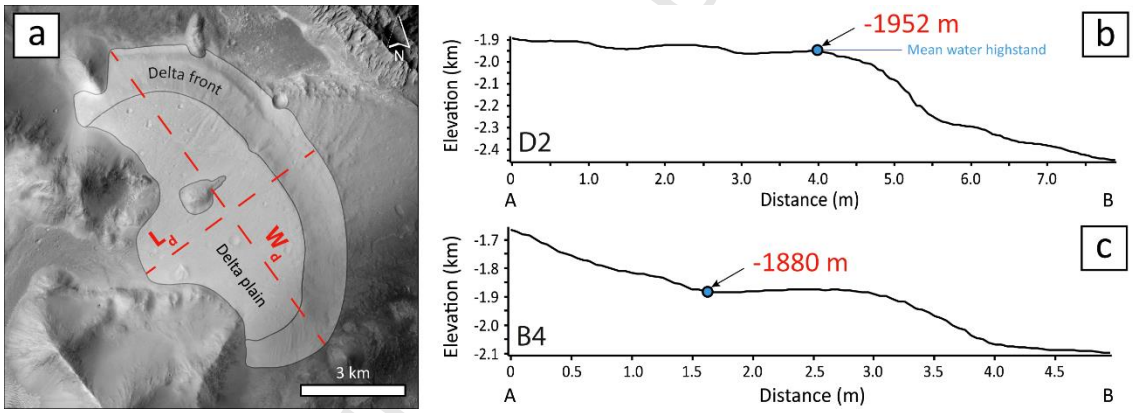

Fig. 2. (a) CTX image of the D2 feature showing the mapped delta plain and front as well as the morphometric parameters L_d (length) and W_d (width) used to calculate the delta-shape index (S_d). (b) and (c) Topographic profiles corresponding to delta D2 and bench B4, respectively (see trace of profiles in Fig. 3). The arrows and blue dots indicate the slope break of the topographic profile used to infer the past water-level elevation from fan-shaped features and benches, as described in the text.

4. Results and discussion

4.1 Description of the fan-shaped and bench-like landforms

We analyzed ten fan-shaped features and fifty-four coastal-like benches. Fan-shaped landforms (labelled as D# in Fig. 3) occur at the mouth of past high-gradient rivers that used to debouch into an unconfined low-lying area. The majority of fan-shaped deposits are linked to drainage basins characterized by poorly-ranked stream networks (Lw). In contrast, D3 and D6 seem to be the only fan-shaped landforms associated with steep canyons (C). These features are distributed along a NW-SE oriented belt associated with the southern margin of interconnected depressions with latitude and longitude coordinates that range from 0°18'8"N to 3°5'31"N and from 121°20'54"E to 127°34'00"E, respectively. The fan-shaped features range from ~3.0 km^2 to ~85.4 km^2 in area and display two well-differentiated parts: low-gradient plains with mean slopes from ~2.3º to ~5.2º, and steep fronts with variable preservation conditions and average gradients from ~3.4º to ~15.8º (see Table 1). The more degraded fan-shaped features (i.e., D1a, D1b and D8), display a lower gradient difference (<2º) between the plains and their fronts, probably due to erosion in the upper part of the slope and accumulation in the footslope (Table 1). In some cases, the plains are dissected by small and rather subdued channels as illustrated in Fig. 5b. The measurement of the width (W_d) and length (L_d) allowed the calculation of the delta-shape index (S_d) for each feature, which ranges between 0.56 (prolate geometry) and 1.02 (oblate geometry). These values are analogous to those from protruding deltas on Earth (e.g., Mikhailova, 2015). Most features display visible layering on their fronts, strongly suggesting that they are formed by stratified sediments (Fig. 5a). The lack of visible or unambiguous layering in some features may be related to a topographic surface concordant with the bedding, as is

commonly the case in delta fronts (dip slope) (e.g., Hampson and Storms, 2003), or to the presence of eolian dust and sand. In the cases where layering is exposed in the front of the delta due to erosion, the slope probably does not represent the foreset inclination. The majority of the features have one defined lobe, whereas D1b, D7 and D9 show two clear lobes, and D2 has two probable frontal lobes, although very poorly defined (Figs. 3 and 5b). These multi-lobe features

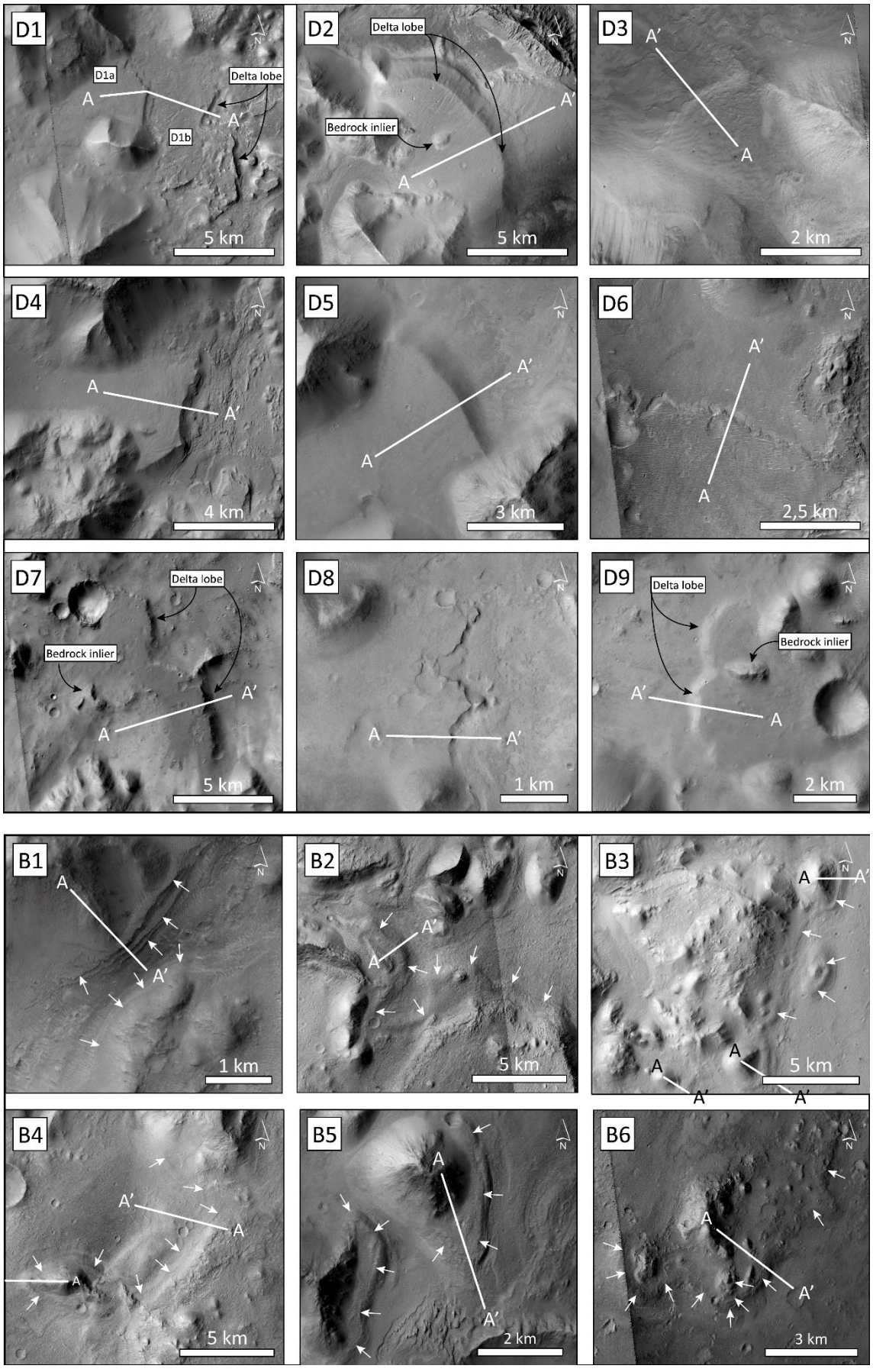

Fig. 3. CTX images illustrating features attributable to putative Gilbert-type deltas and

shore platforms in the study area (labelled as D# and B#, respectively). A-A' lines indicate the trace of the topographic profiles used to infer the mean water level from each feature (Fig. 8). White arrows indicate laterally continuous benches (e.g., B1, B4), some of them associated with residual relief and showing rounded geometry in plan view (e.g., B2, B3, B5 and B6).

have in common the presence of bedrock inliers, likely relict relief that protrudes over their plains. Most of the features show a steep front with a continuous slope (M1). However, D1 displays a stepped front with benches and slope breaks (M2) (Fig. 3).

The coastal-like benches are generally located along the margins of the depressions and encircling isolated massifs and knobs within the depressions. These features have not been identified outside the depressions. A selection of them are shown in Fig. 3 (labelled as B#) and in Fig. 5d. These benches display smooth, subhorizontal or gently-sloping surfaces, with lateral continuity, elevation consistency, and steep slopes associated with their outer edges. In some cases, such as B1 (B1 in Fig. 3), paired benches occur on both sides of the depression at consistent elevation. The relationship between the coastal-like benches and putative deltas is analyzed from their elevation values and spatial distribution (Fig. 8).

Delta	Latitude (N)	Longitude (E)	Delta front elevation (m)	W_d (m)	L_d (m)	Delta-shape index	Mean plain slope (°)	Mean front slope (°)	Visible layering	Multi-lobate	Stepped morphology	Drainage network	Drainage area (km^2)	Delta area (km^2)	First reference
D1a	3°5'31"	121°20'54"	-1865	3627	2971	0.61	4.18	6.05	✓	✗	M2?	Lw	1510.37	7.76	García-Arnay et al. (2018b)
D1b	3°4'30"	121°23'59"	-1972	11124	5529	1.01	4.07	5.44	✓	✓	M2?	Lw	1510.37	40.49*	García-Arnay et al. (2018b)
D2	2°10'11"	121°39'29"	-1952	10430	6045	0.86	3.86	15.38	✓	✓	M1	Lw	20268.25	41.13	Irwin et al. (2005)
D3	2°1'28"	122°00'31"	-1935	2371	1885	0.63	5.19	8.68	✓	✗	M1	C	113.19	2.98	García-Arnay et al. (2018b)
D4	1°34'7"	123°22'52"	-1793	5602	2844	0.98	4.77	14.41	✓	✓	M1	C/Lw	28000.94	10.91*	García-Arnay et al. (2018b)
D5	0°44'6"	125°18'55"	-1920	4740	3500	0.68	2.34	15.82	✓	✗	M1	Lw	8189.85	11.93	García-Arnay et al. (2018b)
D6	0°36'33"	125°47'50"	-1975	4704	2304	1.02	2.95	5.64	✗	✗	M1	C	1908.04	8.53	García-Arnay et al. (2018b)

D7	0°3'14"	126°36'20"	-1186	12621	11069	0.57	3.41	7.76	✓	✓	M1	Lw	156377.80	85.40	García-Arnay et al. (2018b,c)
D8	0°31'21"	126°58'19"	-1920	2458	2176	0.56	2.66	3.40	✓	✓	M1	Lw	-	3.65 *	García-Arnay et al. (2018b)
D9	0°18'8"	127°34'00"	-1783	5424	3520	0.77	3.49	7.56	✗	✓	M1	Lw	10753.31	12.55	García-Arnay et al. (2018b)

Table 1. Morphometric and morphological parameters of the fan-shaped features and their associated drainage networks. (*) Delta surface presents ambiguous and/or eroded limits; (-) no flow accumulation data available to derive the drainage area. Mean slopes correspond to those of the current topographic surface. In the cases where layering is exposed in the front of the delta due to erosion, the slope probably does not represent the foreset inclination. Latitude and longitude coordinates correspond to the point along the topographic profile used to extract the elevation of the delta front (see Fig. 8).

4.2 Spectral analysis of the delta deposits

We carried out the spectral analysis of the CRISM scene FRT000064CE in order to identify possible hydrated minerals. The spectral analysis of this CRISM scene has been also performed by Ehlmann and Buz (2014, 2015). The observation displays a fan-shaped deposit located east of the study area, at the mouth of a valley carved into the southwest side of the Robert Sharp crater rim, east of the study area (Fig. 1a). This deposit was interpreted as fan delta by Irwin et al. 2004 (Fig. 4a). The PHY spectral parameter map reveals that the scene is dominated by hydrated Fe/Mg-phyllosilicates (Ehlmann and Buz, 2015), the most common hydrated minerals on Mars (Carter et al., 2013), as highlighted by the pink-colored pixels in Fig. 4b. The ratioed I/F spectrum (i.e., s1/s2) shows a subtle absorption band feature at ~1.4 μm due to structural H_2O and OH, a sharp absorption feature at ~1.9 μm indicating structural H_2O, as well as an absorption band at ~2.31 μm related to Fe/Mg-OH bond and a subtler band at ~2.39 μm also related to these bonds (Ehlmann et al., 2009; Viviano-Beck et al., 2014) (Fig. 4c). Absorption features are consistent with the presence of saponite (Mg-rich smectite) and nontronite (Fe-rich smectite), as shown by the comparison between the ratioed spectrum and laboratory spectra (Viviano-Beck et al., 2015). These ferromagnesian smectites occur in light-toned layered deposits with apparently meter-scale polygonal fractures along the delta front and at its foot, as revealed by the HiRISE image PSP_001884_1750 (close-up view in Fig. 4a). Clay minerals may either have formed during transport or by near-surface weathering and subsequently transported and deposited as detrital particles (Ehlmann and Buz, 2014).

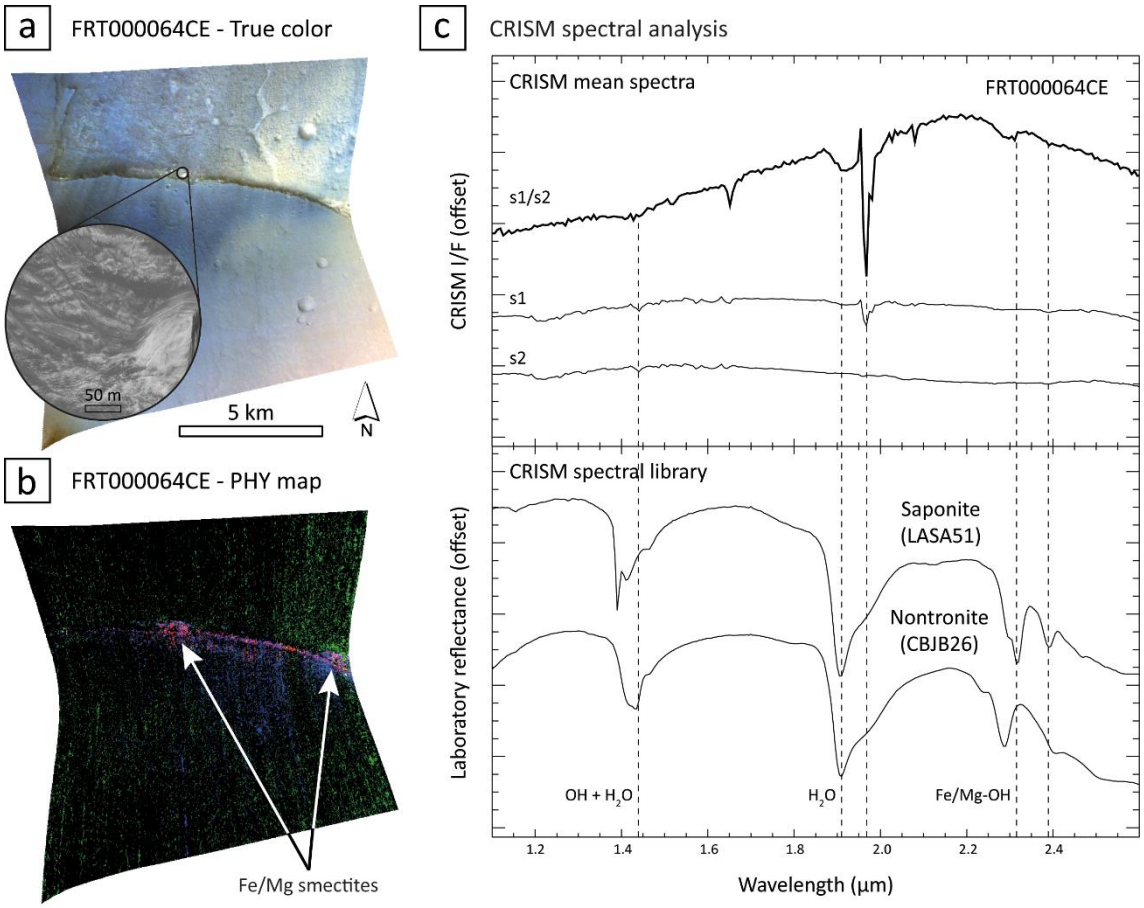

Fig. 4. (a) True color image of the CRISM scene FRT000064CE. The close-up view shows a detail of the light-toned layered deposits occurring at the delta front. (b) Spectral parameter map (PHY product) for the same scene. Pink tones indicate the presence of Fe/Mg- phyllosilicates outcropping along the delta front. (c) CRISM ratioed I/F spectrum compared to CRISM library spectra (vertical dashed lines indicate observed absorption band features).

Other minerals within Robert Sharp crater such as carbonates and akaganéite, which is an oxide mineral related to acidic and oxidizing conditions in a drying lagoon, were reported by Carter et al. (2015). Clay-bearing layered deposits support the presence of liquid water in the past (e.g., Poulet et al., 2005), and are considered potential sites for organic matter preservation due to relatively rapid burial (e.g., Ehlmann et al., 2008).

We consider that these findings strengthen the possible deltaic origin of this fan-shaped deposit and its composition could be analogous to deltas in the study area.

4.3 Interpretation of landforms

Based on the morphologic and morphometric characteristics of the described landforms,their spatial distribution, and spectral analysis, we interpret the fan-shaped features as putative relict Gilbert-type deltas linked to the mouth of drainage basins. The interpreted deltas show an overall convex and segmented longitudinal profile, whereas alluvial fans are characterized by continuous concave long profiles. Furthermore, the presence of steep fronts hundreds of meters in local relief is strongly inconsistent with the interpretation of these features as alluvial or fluvial fans and argues for the presence of a deep water body. Nonetheless, the mapped deltas are expected to have a proximal subaerial component, and as such could be also designated as fan-deltas (Blair and McPherson, 1994).

Some of the ten putative deltas analyzed in this work also have been documented by other authors (e.g., Irwin et al., 2005; de Pablo and Pacifici, 2008; Rivera-Hernández and Palucis, 2019). On Earth, Gilbert-type deltas, which were first described by Gilbert (1884), typically occur in lakes where the near-shore water is relatively deep (e.g., Bird, 2011), and tend to be associated with homopycnal flows (e.g., Penland and Kulp, 2005), in which the density of the river water is very similar to that of the standing mass of water in the basin (Bates, 1953). These flows commonly occur in lacustrine environments and produce rapid deposition to form deltas characterized by steep delta fronts (Figs. 5a, b,

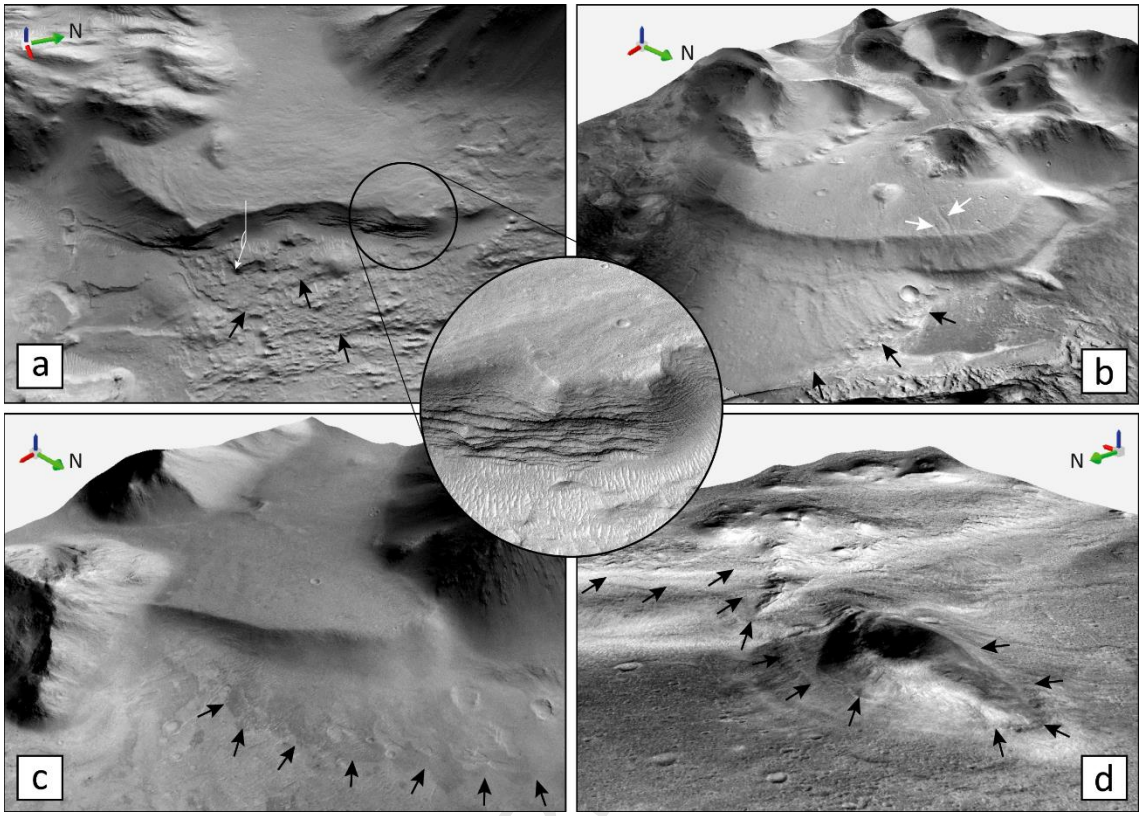

Fig. 5. 3D oblique views of some fan-shaped and coastal-like features (CTX images). (a) The D4 feature shows a steep front scalloped by a long-runout landslide in its central part, which permits observation of inner layering or clinoforms (circle: close-up view of HiRISE image ESP_058612_1815). Note that the lateral extent of the concave headscar of the landslide matches with the hummocky terrain situated at the foot, attributable to a blocky landslide deposits (black arrows). (b) The D2 feature shows two overlapping morpho-stratigraphic units. The oldest apron (foot indicated by black arrows) is partially overlain by the younger one, whose upper plain is carved by subtle channels (white arrows). (c) The D5 feature may also record several phases of development as suggested by the low-albedo apron located at the foot of its front (black arrows). (d) Laterally continuous benches corresponding to B4 at different elevations (black arrows)

around a residual relief, which apparently connected to the "mainland" resembling an older isthmus and a peninsula.

c). Some deltas show multi-lobate fronts (e.g., D1b, D2, D7 and D9, Fig. 3) that may indicate flow bifurcation and/or channel avulsion processes. The presence of bedrock inliers protruding through their plains probably controlled flow bifurcation and the consequent development of two lobes. Deltas D4 and D8 display two apparent lobes, although their shape is probably related to post-depositional landsliding (D4, Fig. 5a) and/or erosion (D8, Fig. 3). The origin of the stepped topography of some delta fronts (D1, Fig. 3) could be either related to erosional benches developed during stages of relatively stable water level that punctuated the overall regression trend, or to differential erosion. Kraal et al. (2008) ascribed the stepped longitudinal profile of an alluvial fan, comprising a sequence of risers and treads, to the episodic decline of the water level and the development of benches during periods of stability. Finally, the possible deltaic origin of the fan-shaped deposits in Nepenthes Mensae is strengthen by the occurrence of phyllosilicate minerals in the front of the analyzed delta, which supports the presence of liquid water in the past.

Based on the morphologic characteristics of the described landforms, their spatial distribution, altitudinal relationship with the deltas, and resemblance with possible terrestrial analogues, we interpret the benches as possible shore platforms developed by coastal erosion along paleoshorelines at different water-level elevations. Shore platforms with rounded outer edges in plan view located around isolated massifs and knobs are common in the northern lowlands, as indicated by Parker et al. (1993). These "stepped massifs", such as those located in Cydonia Mensae, display the same

characteristics as the ones described in this work at Nepenthes Mensae (Parker et al., 1993; Parker and Currey, 2001). Parker et al. (1989, 1993) interpreted these features as possible wave-cut island formed by coastal erosion of the pre-existent rocks during highstands of an ancient liquid-water ocean and/or by erosional processes associated with the floating sea ice on a frozen ocean that occupied the northern lowlands of Mars (Clifford and Parker, 2001). The formation of wave-cut platforms implies that the available fetch, the atmospheric pressure, and wind speed were sufficient to produce these erosional landforms (e.g., Kraal et al., 2006; Bandfield et al., 2015). On Earth, lakes with less than 50 km of open water are considered 'fetch-limited' (e.g., Nordstrom and Jackson, 2012). Eolian landforms developed in the largest depression of Nepenthes Mensae after its desiccation such as dune fields, yardangs and wind streaks indicate predominant NW- and NE-oriented winds. Based on the dimensions of the reconstructed paleolakes (Fig. 9) and the inferred wind directions, fetch values would range from ~40 km to ~100 km. These values are similar to those estimated for the Carson Desert sub-basin of the pluvial Lake Lahontan, United States, during the Pleistocene highstand, ranging from ~50 km to ~110 km (Morrison, 1964). As explained below, this pluvial paleolake displays well-developed shore platforms. Nonetheless, the estimation of the effective fetch of the inferred paleolakes would require to know the predominant wind direction when the erosional benches were formed. Moreover, the unknown erodibility of the materials exposed in the coastal areas play a critical role in the development of these landforms. Alternative processes have been proposed to explain the formation of benches and stepped massifs in other regions of Mars, including differential erosion in layered bedrock (e.g., Carr and Head, 2003) and eolian erosion (e.g., Manent and El-Baz, 1986). Kraal et al. (2006) proposed alternative processes for the development of Martian landforms interpreted as 'bedrock

shoreline features' such as the erosional action of ice in the surface of lakes or seas. An ice-covered lake was also the preferred hypothesis of Howard and Moore (2004) to explain the formation of benches and scarps in the Gorgonum Basin. Sholes et al. (2019) indicate that lineaments and terraces in Cydonia Mensae, which are considered as one of the better candidates for putative paleoshoreline features in the literature, do not show lateral or altitudinal consistency. Consequently, Sholes et al. (2019) considered that those landforms better resemble eroded and exposed bedding surfaces. These interpretations seem to be highly unlikely in our study area since the benches do not show any lithostratigraphic control or any preferred orientation.

4.4 Chronology of the delta and paleolake systems

The surface age of the delta D7 and of the main depression were calculated using crater-size frequency distribution statistics. This delta was selected due to its large area (~80 km^2) in order to reduce uncertainties on the age model (e.g., Warner et al., 2015). We obtained average age estimates of ~3.88 Ga (Middle Noachian) for the delta D7 (Figs. 6a, b), and ~3.71 Ga (Late Noachian) for the depression, considering a counting area of ~6,200 km^2 in the latter (Figs. 6c, d). Both ages are consistent with those assigned to the geological units where these features are located and/or genetically related. According to Tanaka et al. (2014), the deltas associated with the drainage networks occur in the mNh unit (Middle Noachian), and the depressions in the HNt unit (Late Noachian-Early Hesperian). In spite of the age consistency between delta D7 and the depressions, the age model for delta D7 may present more uncertainties than that for the depressions. Its lower counting area (~80 km^2) can imply a higher spatial variability in cratering processes, as well as the exclusion of larger craters (Warner et al., 2015).

Furthermore, the significant higher elevation of the delta D7 with respect to other deltas in the study area and the depressions do not permit confidence in associating its age with them.

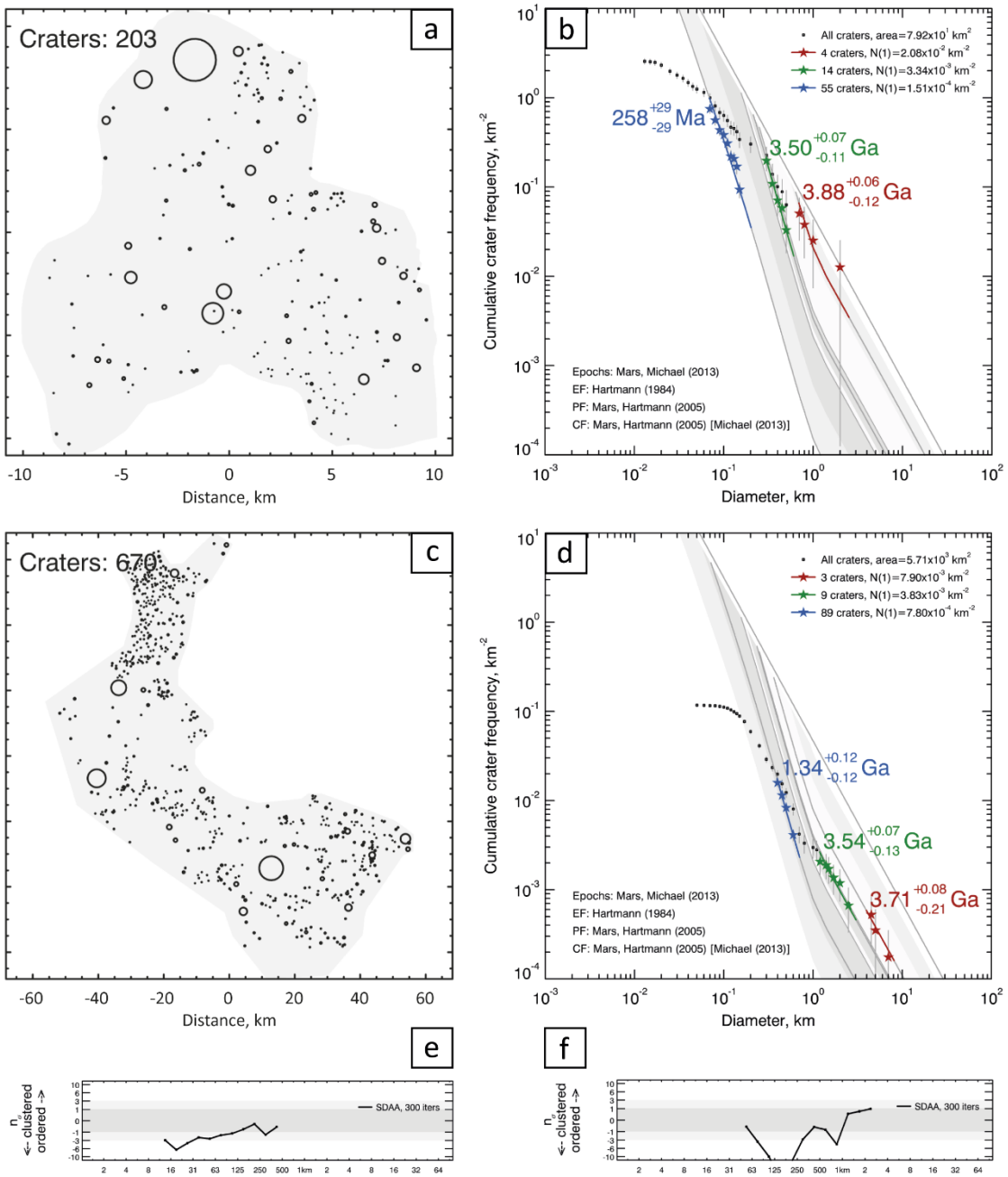

Fig. 6. (a, c) Crater-counting areas used for estimating the numerical age of delta D7 and the main depression, respectively (see location in Fig. 1c). (b, d) Age models

showing simple cumulative fit for the formation age (red fit line), and corrected cumulative fits for the resurfacing events (green and blue fit lines) of the delta D7 and the main depression, respectively. The grey shadow bands represent the boundaries between the different Martian geological epochs (Michael, 2013). (e, f) Randomness analysis for the crater population of the delta and the depression, respectively.

According to Brossier et al. (2015), the estimated age of the delta located at the southwestern part of the Robert Sharp crater (Fig. 1a) is ~1.30 ± 0.37 Ga (Early Amazonian), with delta front elevation at around -2,400 m, and an area of ~120 km^2. The remarkable age difference between the delta D7 and that located at the Robert Sharp crater could be either related to different formation ages or to resurfacing events associated with possible later aqueous phases that would have obliterated the oldest craters on the delta at Robert Sharp crater. Ejecta deposits related to an impact crater 23 km in diameter seems to obstruct the outlet of the ancient fluvial valley of Licus Vallis. These ejecta deposits probably prevented the fluvial reactivation of delta D7. Additionally, according to Warner et al. (2015), the selected area for confidently assessing the age of a surface should exceed 1,000 km^2, whereas the mentioned deltas have significantly smaller areas.

The randomness analysis reveals that the clustering trend of the crater population in the main depression is significantly larger than in the delta, which is more ordered (Figs. 6a, e), with craters ranging from around 100 m to 300 m in diameter in the depression (Figs. 6c, f). Several resurfacing events have been identified, one of them affecting both features ~3.5 Ga ago (Early Hesperian), probably related to late episodes of aqueous activity (Figs. 6b, d). In summary, the chronological analysis indicates that

(1) fluvial-lacustrine processes occurred in the region during the Noachian; and (2) the later occurrence of resurfacing events probably related to renewed flooding during the Early Hesperian or later.

4.5 Terrestrial analogs

In order to compare the putative paleolakes and the associated coastal-like features of Nepenthes Mensae with analog landforms on Earth, we focused our attention on Lake Bonneville and Lake Lahontan, two large and deep pluvial lakes that used to be located in the Great Basin of western North America during the Pleistocene (e.g., Broecker and Orr, 1958). Lake Lahontan and Lake Bonneville reached their maximum water level around 15 kyr ago during the Late Pleistocene, covering areas of 22,300 km^2 and 51,300 km^2, respectively (Benson et al., 2011). These paleolakes, partially desiccated at the present time, and their relict landforms (e.g., wave-cut platforms, beach ridges, spits, barriers, bars) have been proposed as terrestrial analogs for putative ancient lakes and oceans on Mars by multiple authors (e.g., Clifford and Parker, 2001; Zimbelman et al., 2004, 2005; Parker et al., 2010; Irwin and Zimbelman, 2012;). We chose these pluvial paleolakes for comparison with our study area due to the following reasons: (1) the presence of well-preserved paleoshorelines recorded by laterally continuous shore platforms and beach ridges developed at different water-level elevations (Figs. 7b, c) (e.g., Oviatt, 2015); (2) these relict coastal features resemble those identified along the edges of the depressions and around the residual reliefs in Nepenthes Mensae (Fig. 7a); (3) the presence of multiple former deltas located at the mouth of fluvial valleys such as the Bonneville-level delta at American Fork (Godsey et

al., 2005), which was first analyzed by Gilbert (1890); (4) these coarse-grained deltas (Gilbert-type deltas) were fed

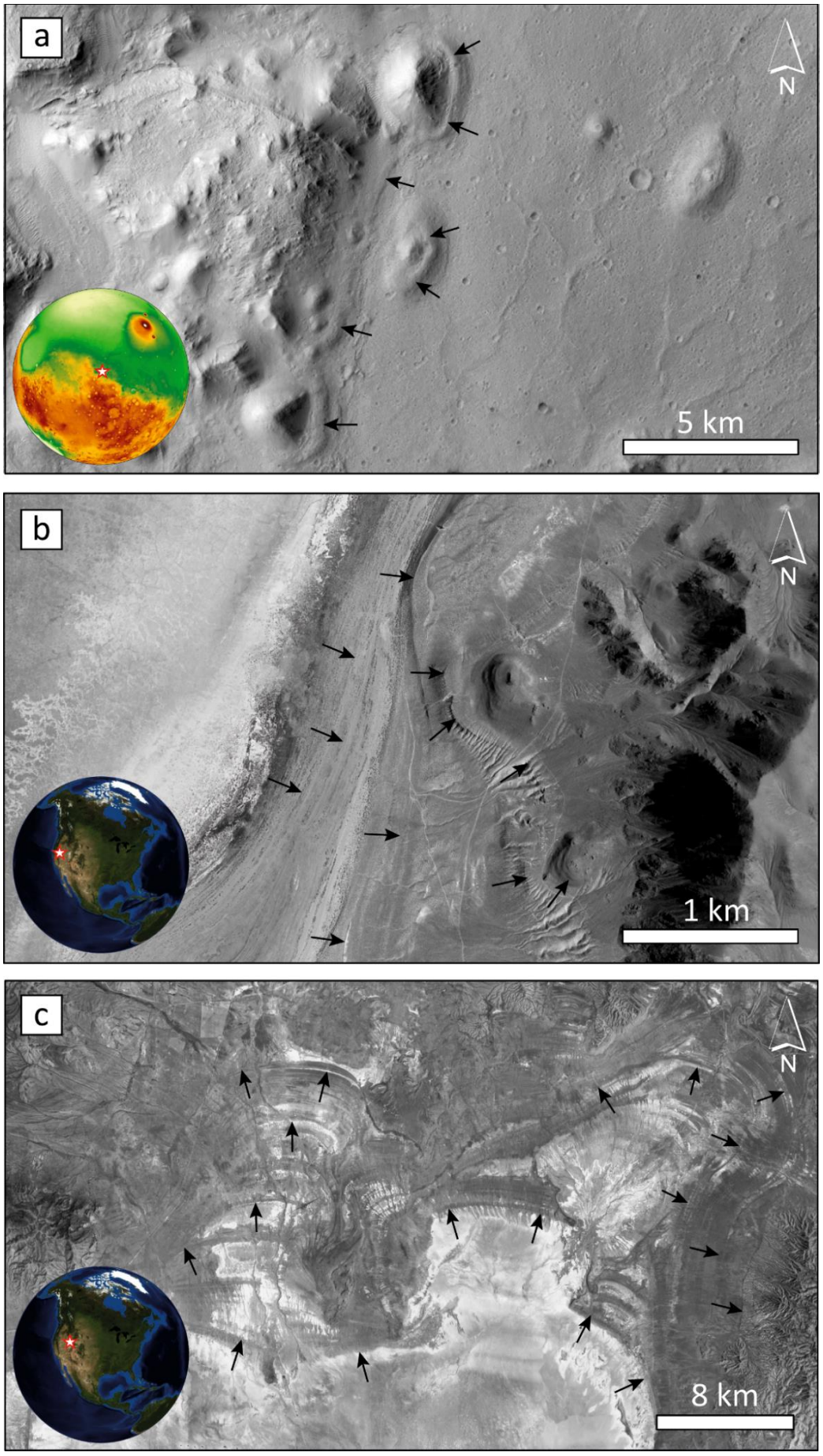
a
N
5 km
b
N
1 km
c
N
8 km

Fig. 7. (a) Comparison between the putative coastal landforms in Nepenthes Mensae (Mars, image centered at 2°24'2"N, 124°44'10"E), and (b) those in terrestrial paleolakes such as Lake Lahontan (Nevada, USA; image centered at 40º14'3"N, 119º17'4"W) and (c) Lake Bonneville (Utah, USA; image centered at 41º29'55"N, 113º25'53"W). Arrows point to laterally continuous benches with consistent elevation and strandlines that record paleowater levels (Images from CTX and Google Earth).

by high-gradient rivers associated with canyons and small watersheds (Lemons and Chan, 1999); (5) both terrestrial paleolakes are located within endorheic basins as seems to be the case of those in Nepenthes Mensae; and (6) the extent covered by the Lake Lahontan during its highstand (22,300 km^2) is comparable to the sum of the surface areas of the paleolakes in Nepenthes Mensae during the mean highstand yielding a total area of ~19,000 km^2 (Fig. 9).

The strong resemblance (i.e., morphology, morphometry, spatial relationships) between the analyzed landforms on Mars and the terrestrial analogs is used to support our geomorphic and paleohydrologic interpretations.

4.6 Paleohydrological reconstruction

Elevations extracted from the putative deltas and shore platforms occur within the elevation ranges -1,186 m to -1,975 m, and -1,811 m to -2,150 m, respectively (Fig. 8). Elevation values are rather scattered and collectively do not define a clear equipotential surface. This fact can be related to several disconnected water bodies and multiple water levels. Delta fronts yield a mean elevation of -1,830 m (standard deviation of 236 m). If

the anomalous elevation of D7 is not considered, delta fronts yield an average elevation of -1,902 m (standard deviation of 72 m). Collectively, benches yield a mean elevation value of -1,978 m (standard deviation of 57.6 m). Deltas and benches associated with the main paleolake (i.e., deltas D2, D3, D5, and D6; and forty-four out of the fifty-four benches) yield mean elevations of -1,946 m (standard deviation of 24 m) for deltas, and -1,986 m (standard deviation of 56 m) for benches (see dashed lines in Fig. 8). The mean elevations among deltas and benches are consistent and define a contour along the edges of the depressions. In addition, these mean elevations are coherent with the average elevation of deltas within the main paleolake obtained by Rivera-Hernández and Palucis (2019), whose value is -1,934 ± 33 m. These authors used two deltas documented within the main paleolake (deltas D2 and D5, as are identified in our work) for calculating that average elevation. It seems to correspond to a paleowater level of a former inland sea or of a series of interconnected lakes with sufficient persistence to have a significant geomorphic imprint in the landscape. Using the mean elevation value from deltas of the main paleolake (around -1,950 m), we have reconstructed the paleogeography of the paleolakes that used to occupy the depressions of Nepenthes Mensae (Fig. 9). According to this reconstruction, the largest paleolake reached an area of ~12,787 km^2, an estimated water volume of 3,648 km^3, and mean and maximum depths of ~290 m and ~1,000 m, respectively. Estimations for the area of the largest paleolake and its volume are similar to those calculated by Rivera-Hernández and Palucis (2019), whose values are 12,830 km^2 and 3,890 km^3, respectively. The sum of the areas of the paleolakes in Nepenthes Mensae reached ~19,000 km^2 during the mean highstand. The surface of the depressions below the reconstructed paleolake level show a smoother surface than that located above this level and outside the basin. This morphological feature, which is also observed in terrestrial paleolakes such as Lake

Bonneville and Lake Lahontan, may be attributed to sediment aggradation in the bottom of the paleolakes and exposure to erosional processes during a shorter time span, after the desiccation of the lakes.

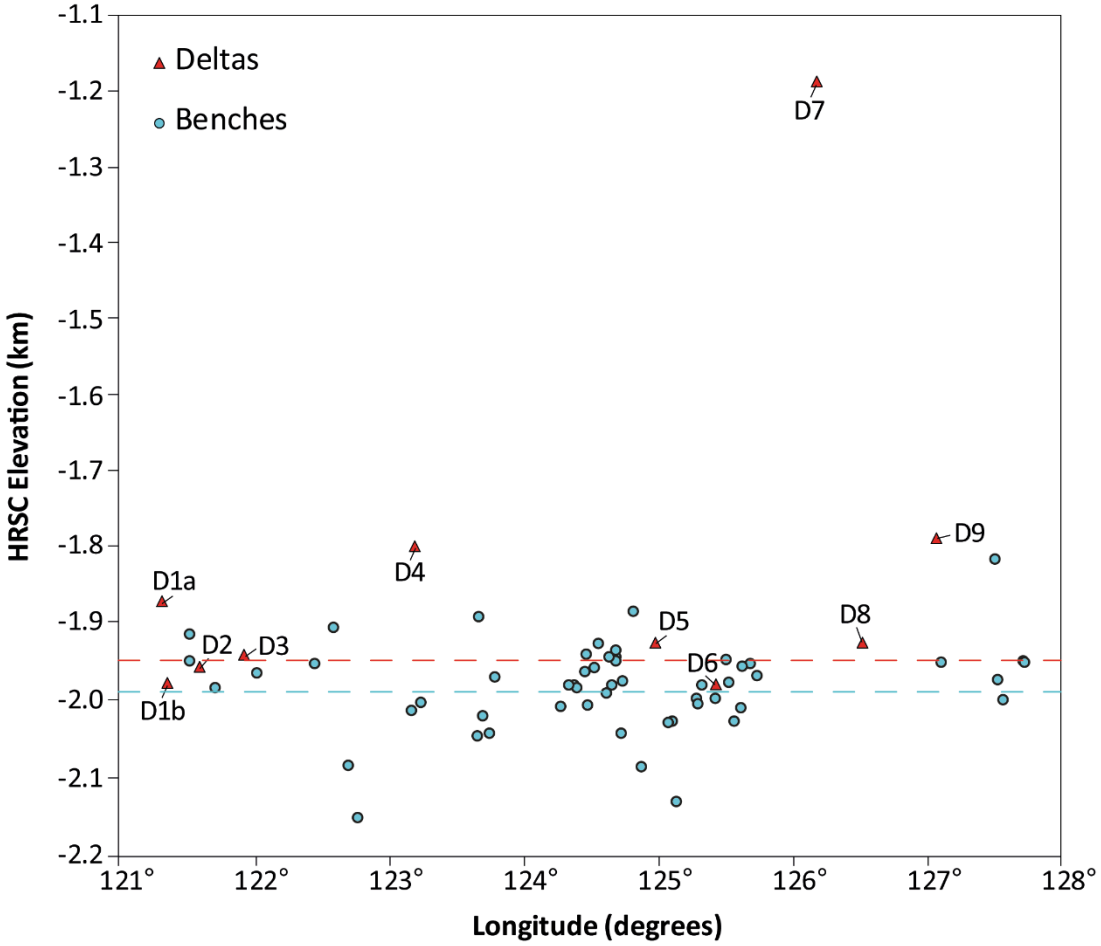

Fig. 8. Elevation values from each putative delta (plain-front junction, Table 1) and shore platform (inner edge) used to infer the past water levels. The dashed red and blue lines indicate, respectively, the mean elevation for deltas and shore platforms situated within the main paleolake. Note that delta D7 is located at an anomalous elevation compared with the rest of measured coastal landforms.

The deltas associated with the main depression (i.e., D2, D3, D5 and D6) show consistent delta-front elevations. However, the elevation of the front of the majority of

the deltas that are not spatially associated with the main depression do not fall within their elevation range (i.e., D1a, D4, D7, and D9), with the exception of D1b and D8. Deltas D1a, D4, D7 and D9 show delta front elevations above -1,900 m. This fact may be due to different water-level elevations. We propose that the anomalous elevation of delta D7, which is the largest of the study area (~85 km^2), is related to the presence in the past of a small enclosed depression at the mouth of Licus Vallis, perched above and disconnected from the main system of depressions, with a local base level located at an elevation of around -1,200 m (Fig. 8). A small valley occurs below this inferred basin, which may receive two non-excluding interpretations: (1) an overflow channel of the depression; (2) the stream that captured the perched depression. The delta D8 occurs at the mouth of this valley at an elevation of around -1,920 m, which is consistent with the mean water level calculated for deltas of the main paleolake. The anomalous elevation difference (~720 meters) cannot be explained by differential vertical displacements due to the lack of discrete tectonic structures between deltas D7 and D8, situated ~34 km apart (Fig. 10). Black et al. (2017) proposed that regional tectonic activity was low during the period of formation of valley networks on Mars, and Goudge and Fassett (2018) inferred that regional uplift was not an important factor during the configuration of the drainage network of Licus Vallis. Therefore, we consider that the present topography is similar to what existed during the incision of the drainage network and the development of the deltas.

Multiple "levels" interpreted as paleoshorelines have been identified on Mars (e.g., Carr and Head, 2003; Webb, 2004; Ghatan and Zilbelman, 2006). The "Contact 1", defined by Parker et al. (1989), and renamed as "Arabia shoreline" by Clifford and Parker (2001), is the topographically highest level of the putative Martian ocean, which

shows significant elevation variations along the northern plains of up to several kilometers,

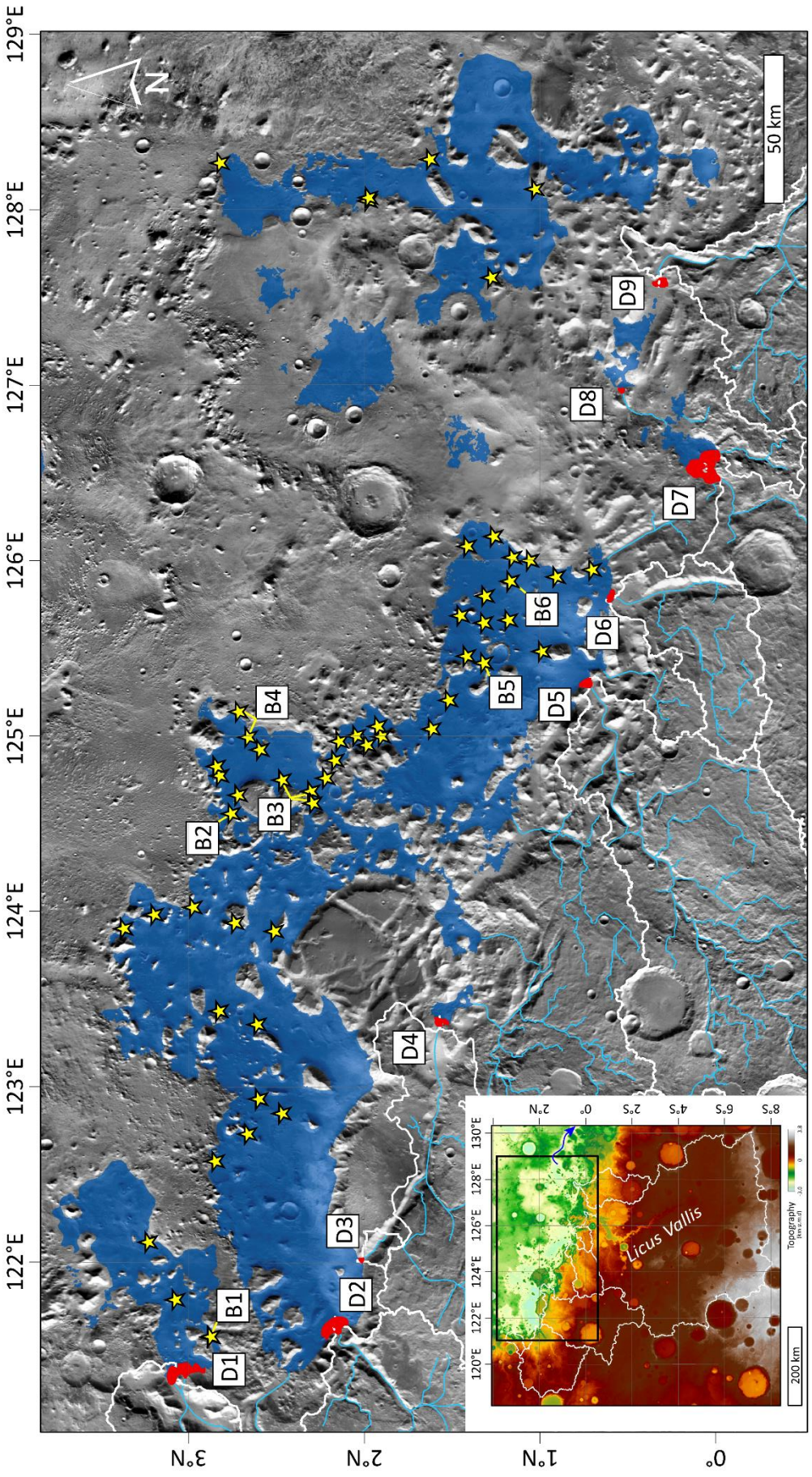
N
50 km
B1
B2
B3
B4
B5
B6
D1
D2
D3
D4
D5
D6
D7
D8
D9
Licus Vallis
200 km
Topography
122°E
123°E
124°E
125°E
126°E
127°E
128°E
129°E
3°N
2°N
1°N
0°

Fig. 9. Inset: elevation model of the study area showing the watershed boundaries (white lines) and the area depicted in the overview (black polygon). The blue arrow indicates that the depressions probably used to connect eastward with the northern lowlands (HRSC-MOLA blended topography). Overview: paleogeographic reconstruction of the paleolakes (blue polygons), based on the mean elevation (~-1,950 m) of the paleo-water level recorded by the putative deltas of the main paleolake. Deltas and shore platforms are indicated by red areas and yellow stars, respectively. The stream network is represented with light-blue lines. The labels indicate the location of the images shown in Fig. 3 (base map mosaic from THEMIS-IR day images).

attributable to subsequent regional deformation caused by true polar wander (Perron et al., 2007). Achille and Hynek (2010) inferred an equipotential surface (referred to as "S"level) from elevation values of 17 putative delta fronts located in open basins along the margins of the Martian lowlands. This level lies at a mean elevation of -2,540 m (standard deviation of 177 m), which is consistent with the mean elevation inferred for the Arabia level (-2,499 m) (Clifford and Parker, 2001; Achille and Hynek, 2010). This level is ~500 m lower than the one inferred in this work at Nepenthes Mensae (around -1,950 m) from putative deltas of the main depression. However, these deltas were probably associated with an endorheic basin occupied by an inner sea or large interconnected paleolakes. It is possible that, at some stage, these basins became connected to the putative Oceanus Borealis before the water level dropped, supported by the fact that the depressions connect eastward to the northern lowlands (Fig. 9). However, this possible connection to a northern ocean would require a more detailed investigation.

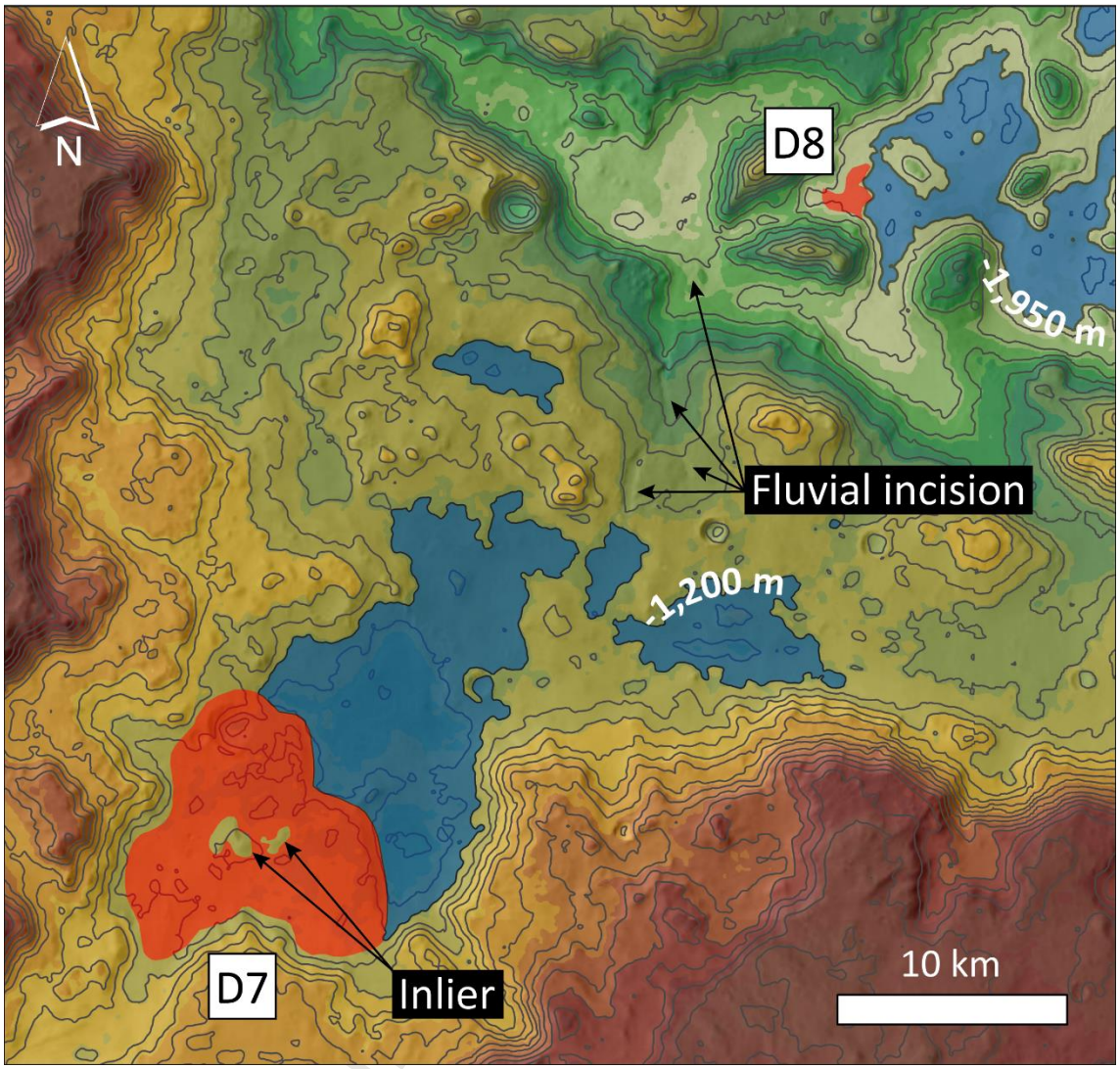

Fig. 10. Context map with 100 m contour lines showing the spatial-altitudinal distribution of deltas D7 and D8 (red polygons), as well as the respective paleolakes (blue polygons). Delta D7 includes interior high points likely representing bedrock inliers, which probably controlled the formation of two delta lobes (CTX mosaic over HRSC topography).

4.7 Geomorphological history

In order to summarize the geomorphological evolution of the study area, focusing on the history of the paleolakes, we propose the following possible sequence of events: (1) The large depressions that hosted the paleolakes were formed along the dichotomy boundary during the Noachian. The origin of these basins could be related to various types of large-scale deformation processes, although it remains uncertain. (2) Fluvial processes initiated with the presence of liquid water and runoff resulted in the development of valleys carved into the mNh unit in the highlands. These N-directed drainage systems fed the paleolakes developed in the endorheic depressions located along the dichotomy. (3) The presence of long-standing water bodies and relatively long periods of lake-level stability permitted the formation of deltas at the mouth of the valleys and coastal benches along the margins of the depressions and around residual reliefs. (4) The paleolakes probably experienced a long-term water-level decline punctuated by periods of stability, as supported by inset benches at different elevations. (5) The resurfacing events suggested by the chronological analysis carried out in the bottom of the depressions could be related to new flooding events during the Early Hesperian or later. (6) Finally, hydrological activity in the region declined and as a result the paleolakes desiccated. This situation allows the observation of the relict geomorphic features related to former base levels, as occurs in the proposed pluvial paleolakes as terrestrial analogs. At the present time, the landscape is being modified by depositional and erosional eolian processes as recorded by dune fields and yardangs.

5. Conclusions

The fan-shaped and terrace-like features identified in Nepenthes Mensae are likely relict Gilbert-type deltas and shore platforms, respectively, developed along

paleoshorelines. This interpretation is supported by several lines of evidence: (1) their spatial distribution, with putative deltas linked to the mouth of drainage networks, and benches located along the margins of the depressions and around prominent residual reliefs; (2) their morphological resemblance with other Martian landforms attributed by other authors to relict deltas and markers of paleoshorelines; (3) the lateral continuity along kilometers of the gently-sloping benches; (4) the elevation consistency among the benches and deltas as shown by their altitudinal distribution; (5) the detection of hydrated minerals (Fe/Mg smectites) occurring in the surface of the front of a delta analyzed near the study area, indicative of the existence of liquid water in the past; and (6) the analogy between these ancient Martian landforms and those documented in Pleistocene paleolakes, such as Lake Bonneville and Lake Lahontan, including the extent and endorheic nature of these terrestrial paleolakes and those inferred in Nepenthes Mensae. Assuming that the current regional topography is similar to the one that existed during the development of the analyzed landforms, their elevations permitted us to approximately determine the mean water level at around -1,950 m corresponding to an ancient inner sea or a system of interconnected paleolakes that occupied the belt of NW-SE trending depressions. This past water level is consistent with the mean elevation reported for the mean Arabia level. The paleolakes may have experienced a long-term water-level decline punctuated by periods of stability, as supported by inset benches at different elevations. These findings shed light into the paleogeography and paleohydrologic conditions in the Nepenthes Mensae region during the Late Noachian-Early Hesperian transition. They also contribute to contextualize the continuous findings on the environmental and climatic conditions in nearby Gale crater at a similar time; and illustrates the important morphogenetic role that liquid water may have played on Mars in the past.

Acknowledgments

This research was supported by a PhD scholarship granted to ÁG-A (C237/2016) by the Gobierno de Aragón (Spain) and the European Social Fund, by project CGL2017-85045-P (Ministerio de Ciencia, Innovación y Universidades, Gobierno de España), and by the Ibercaja-CAI mobility program (CB 5/18) funded by Universidad de Zaragoza, Fundación Bancaria Ibercaja y Fundación CAI (mobility funding for research stay of Á.G-A. at the Centro de Astrobiología (INTA-CSIC)). The authors would like to thank Dr. Joel Davis and an anonymous reviewer for their comments and suggestions which helped to improve the paper.

References

Andrews- Hanna, J.C., Phillips, R.J., 2007. Hydrological modeling of outflow channels and chaos regions on Mars. J. Geophys. Res. Planets, 112(E8). doi: 10.1029/2006JE002881.

Baker, V.R., 2001. Water and the Martian landscape. Nature, 412(6843), 228. doi: 10.1038/35084172.

Banfield, D., Donelan, M., Cavaleri, L., 2015. Winds, waves and shorelines from ancient martian seas. Icarus 250, 368–383. doi: 10.1016/j.icarus.2014.12.001.

Bates, C.C., 1953. Rational theory of delta formation. AAPG Bulletin, 37(9), 2119-2162.

Benson, L.V. et al., 2011. The rise and fall of Lake Bonneville between 45 and 10.5 ka. Quatern. Int., 235(1-2), 57-69. doi: 10.1016/j.quaint.2010.12.014.

Bird, E.C., 2011. Coastal geomorphology: an introduction. John Wiley & Sons. 436 pp.

Black, B.A., J.T. Perron, D. Hemingway, E. Bailey, F. Nimmo, H. Zebker, 2017. Global drainage patters and the origins of topographic relief on Earth, Mars, and Titan, Science, 356, 727–731, doi: 10.1126/science.aag0171.

Blair, T.C., McPherson, J.G., 1994. Alluvial fans and their natural distinction from rivers based on morphology, hydraulic processes, sedimentary processes, and facies assemblages. Journal of sedimentary research, 64(3a), 450-489. doi: 10.1306/D4267DDE-2B26-11D7-8648000102C1865D.

Bibring, J.P. et al., 2006. Global mineralogical and aqueous Mars history derived from OMEGA/Mars Express data. Science, 312(5772), 400-404. doi: 10.1126/science.1122659.

Broecker, W.S., Orr, P.C., 1958. Radiocarbon chronology of Lake Lahontan and Lake Bonneville. Geol. Soc. Am. Bull. , 69(8), 1009-1032. doi: 10.1130/0016-7606(1958)69[1009:RCOLLA]2.0.CO;2.

Brossier, J., Le Deit, L., Hauber, E., Mangold, N., Carter, J., Jaumann, R., 2015. Reconstructing the infilling history within Robert Sharp Crater, Mars: Insights from morphology and stratigraphy. In European Planetary Science Congress Abstracts, vol. 10, EPSC2015-735.

Caldwell, R.L., Edmonds, D.A., 2014. The effects of sediment properties on deltaic processes and morphologies: A numerical modeling study. J. Geophys. Res. Earth, 119(5), 961-982. doi: 10.1002/2013JF002965.

Caprarelli, G., 2015. Stratigraphic relations of Hesperian transition units in the Nepenthes region, Mars. In: Lunar and Planetary Science Conference Abstracts, vol. 46, p#1584.

Carr, M.H., Head III, J.W., 2003. Oceans on Mars: An assessment of the observational evidence and possible fate. J. Geophys. Res. Planets, 108(E5). doi: 10.1029/2002JE001963.

Carter, J., F. Poulet, J.-P. Bibring, N. Mangold, S. Murchie, 2013. Hydrous minerals on Mars as seen by the CRISM and OMEGA imaging spectrometers: Updated global view, J. Geophys. Res. Planets, 118, 831–858, doi: 10.1029/2012JE004145.

Carter, J., Viviano-Beck, C., Loizeau, D., Bishop, J., Le Deit, L., 2015. Orbital detection and implications of akaganeite on Mars. Icarus, 253, 296-310. doi: 10.1016/j.icarus.2015.01.020.

Christensen, P.R., et al., 2004. The thermal emission imaging system (THEMIS) for the Mars 2001 Odyssey Mission. Space Sci. Rev., 110(1-2), 85-130. doi: 10.1023/B:SPAC.0000021008.16305.94.

Christensen, P.R., Fergason, R.L., Edwards, C.S., Hill, J., 2013. THEMIS-derived thermal inertia mosaic of Mars: product description and science results. In: Lunar and Planetary Science Conference Abstracts, vol. 44. The Woodlands, Texas, p. # 2822.

Clifford, S.M., Parker, T.J., 2001. The evolution of the Martian hydrosphere: Implications for the fate of a primordial ocean and the current state of the northern plains. Icarus, 154(1), 40-79. doi: 10.1006/icar.2001.6671.

de Pablo, M.Á., Pacifici, A., 2008. Geomorphological evidence of water level changes in Nepenthes Mensae, Mars. Icarus, 196(2), 667-671. doi: 10.1016/j.icarus.2008.04.005.

de Pablo, M.Á., Pacifici, A., 2009. Chain of depressions and the watershed evolution in Nepenthes Mensae, Mars. In: Lunar and Planetary Science Conference Abstracts, vol. 40, p#1095.

Di Achille, G., Hynek, B.M., 2010a. Deltas and valley networks on Mars: Implications for a global hydrosphere. Lakes on Mars, 223-248. doi: 10.1016/C2009-0-06633-1.

Di Achille, G., Hynek, B.M., 2010b. Ancient ocean on Mars supported by global distribution of deltas and valleys. Nat. Geosci., 3(7), 459-463. doi: 10.1038/ngeo891.

Dickson, J.L., Kerber, L.A., Fassett, C.I., Ehlmann, B.L., 2018. A Global, Blended CTX Mosaic of Mars with Vectorized Seam Mapping: A New Mosaicking Pipeline Using Principles of Non-Destructive Image Editing. In: Lunar and Planetary Science Conference Abstracts, vol. 49, p#2480.

Ehlmann, B.L., Mustard, J.F., Fassett, C.I., Schon, S.C., Head III, J.W., Des Marais, D.J., Grant, J.A., Murchie, S.L., 2008. Clay minerals in delta deposits and organic preservation potential on Mars. Nat. Geosci., 1(6), 355-358. doi: 10.1038/ngeo207.

Ehlmann, B.L., Mustard, J.F., Swayze, G.A., Clark, R.N., Bishop, J.L., Poulet, F., Des Marais, D.J., Roach, L.H., Milliken, R.E., Wray, J.J., Barnouin-Jha, O.S., Murchie, S.L., 2009. Identification of hydrated silicate minerals on Mars using MRO-CRISM: Geologic context near Nili Fossae and implications for aqueous alteration. J. Geophys. Res. Planets, 114, E2. doi: 10.1029/2009JE003339.

Ehlmann, B.L., Buz, J., 2014. Hydrology and Aqueous Alteration in the Watershed of Gale, Sharp, and Knobel Craters: A Regional Context for Curiosity's Exploration. In: Lunar and Planetary Science Conference Abstracts, vol. 45, p#2587.

Ehlmann, B.L., Buz, J., 2015. Mineralogy and fluvial history of the watersheds of Gale, Knobel, and Sharp craters: A regional context for the Mars Science Laboratory Curiosity's exploration. Geophys. Res. Lett., 42(2), 264-273. doi: 10.1002/2014GL062553.

Fawdon, P., Gupta, S., Davis, J.M., Warner, N.H., Adler, J.B., Balme, M.R., Bell, J.F., Grindrod, P.M., Sefton-Nash, E., 2018. The Hypanis Valles delta: The last highstand of a sea on early Mars? Earth Planet. Sc. Lett., 500, 225–241. doi: 10.1016/j.epsl.2018.07.040

Fassett, C.I., Head III, J.W., 2008. Valley network-fed, open-basin lakes on Mars: Distribution and implications for Noachian surface and subsurface hydrology. Icarus, 198(1), 37-56. doi: 10.1016/j.icarus.2008.06.016.

Fergason, R.L, Hare, T.M., Laura, J., 2018, HRSC and MOLA Blended Digital Elevation Model at 200m v2, Astrogeology PDS Annex, U.S. Geological Survey, URL: http://bit.ly/HRSC_MOLA_Blend_v0.

Figueiredo, P.M., Cabral, J., Rockwell, T.K., 2014. Recognition of Pleistocene marine terraces in the Southwest of Portugal (Iberian Peninsula): Evidences of regional Quaternary uplift. Ann. Geophys., 56(6). doi: 10.4401/ag-6276.

García-Arnay, J.Á., 2016. Cartografía geomorfológica de la región de Nepenthes Mensae, Marte: evidencias de un antiguo mar (Master's thesis, Universidad de Zaragoza, Zaragoza, Spain). Retrieved from https://zaguan.unizar.es/record/58648/files/TAZ-TFM-2016-821.pdf.

García-Arnay, Á., Gutiérrez, F., Fernández, S., 2018a. Coastal-Like Features in Nepenthes Mensae, Mars as Paleowater-Level Indicators, and a Terrestrial Analog. In:

Lunar and Planetary Science Conference Abstracts, vol. 49, p#2595. Retrieved from https://www.hou.usra.edu/meetings/lpsc2018/pdf/2595.pdf.

García-Arnay, Á., Gutiérrez, F., de Pablo, M.Á, Fernández, S., 2018b. Characterization and interpretation of the fan-shaped and terrace-like features identified in Nepenthes Mensae, Mars. In: EGU General Assembly Conference Abstracts, vol. 20, p# 808. Retrieved from https://figshare.com/articles/Characterization_and_interpretation_of_the_fan-shaped_and_terrace-like_features_identified_in_Nepenthes_Mensae_Mars/9824609.

García-Arnay, Á., Fernández, S., de Pablo, M.Á., Gutiérrez, F., 2018c. The dominant morphogenetic role of surface runoff in Licus Vallis, Mars: results from geomorphological and morphometric analyses. Geogaceta, 63, 63-66. Retrieved from http://www.sociedadgeologica.es/archivos/geogacetas/geo63/geo63_16.pdf.

Ghatan, G.J., Zimbelman, J.R., 2006. Paucity of candidate coastal constructional landforms along proposed shorelines on Mars: Implications for a northern lowlands-filling ocean. Icarus, 185(1), 171-196. doi: 10.1016/j.icarus.2006.06.007.

Gilbert, G.K., 1884. The topographical features of lake shores. United States Geological Survey Annual Report, 5, 104-108.

Gilbert, G.K., 1890. Lake Bonneville (Vol. 1). US Government Printing Office.

Godsey, H.S., Atwood, G., Lips, E., Miller, D.M., Milligan, M., Oviatt, C.G., 2005. Don R. Currey memorial field trip to the shores of Pleistocene Lake Bonneville. In: Pederson, J. L., Dehler, C. M. (eds.). Interior Western United States. Geological Society of America Field Guide 6, 419-448. doi: 10.1130/2005.fld006(19).

Goudge, T.A., Aureli, K.L., Head, J.W., Fassett, C.I., Mustard, J.F., 2015. Classification and analysis of candidate impact crater-hosted closed-basin lakes on Mars. Icarus, 260, 346-367. doi: 10.1016/j.icarus.2015.07.026.

Goudge, T.A., Fassett, C.I., 2018. Incision of Licus Vallis, Mars, from multiple lake overflow floods. J. Geophys. Res. Planets, 123(2), 405-420. doi: 10.1002/2017JE005438.

Hampson, G.J., Storms, J.E., 2003. Geomorphological and sequence stratigraphic variability in wave- dominated, shoreface- shelf parasequences. Sedimentology, 50(4), 667-701. doi: 10.1046/j.1365-3091.2003.00570.x.

Harrison, K.P., Grimm, R.E., 2005. Groundwater- controlled valley networks and the decline of surface runoff on early Mars. J. Geophys. Res. Planets, 110(E12). doi: 10.1029/2005JE002455.

Hartmann W.K., Neukum G. (2001) Cratering Chronology and the Evolution of Mars. In: Kallenbach R., Geiss J., Hartmann W.K. (eds). Chronology and Evolution of Mars. Space Sciences Series of ISSI, vol 12. Springer, Dordrecht. doi: 10.1007/978-94-017-1035-0_6.

Hartmann, W.K., 2005. Martian cratering 8: Isochron refinement and the chronology of Mars. Icarus 174 (2), 294–320. doi: 10.1016/j.icarus.2004.11.023.

Head, J.W., Hiesinger, H., Ivanov, M.A., Kreslavsky, M.A., Pratt, S., Thomson, B.J., 1999. Possible ancient oceans on Mars: evidence from Mars Orbiter Laser Altimeter data. Science, 286(5447), 2134-2137. doi: 10.1126/science.286.5447.2134.

Hearty, P.J., Hollin, J.T., Neumann, A.C., O'Leary, M.J., McCulloch, M., 2007. Global sea-level fluctuations during the Last Interglaciation (MIS 5e). Quaternary Sci. Rev., 26(17-18), 2090-2112. doi: 10.1016/j.quascirev.2007.06.019.

Howard, A.D., Moore, J.M., 2004. Scarp-bounded benches in Gorgonum Chaos, Mars: Formed beneath an ice-covered lake? Geophys. Res. Lett. 31, L01702. doi: 10.1029/2003GL018925.

Irwin, R.P., Howard, A.D., 2002. Drainage basin evolution in Noachian Terra Cimmeria, Mars. J. Geophys. Res. Planets, 107(E7). doi: 10.1029/2001JE001818.

Irwin III, R.P., Watters, T.R., Howard, A.D., Zimbelman, J.R., 2004. Sedimentary resurfacing and fretted terrain development along the crustal dichotomy boundary, Aeolis Mensae, Mars, J. Geophys. Res. Planets, 109, E09011, doi: 10.1029/2004JE002248.

Irwin, R.P., Howard, A.D., Craddock, R.A., Moore, J.M., 2005. An intense terminal epoch of widespread fluvial activity on early Mars: 2. Increased runoff and paleolake development. J. Geophys. Res. Planets, 110(E12). doi: 10.1029/2005JE002460.

Irwin, R.P., Zimbelman, J.R., 2012. Morphometry of Great Basin pluvial shore landforms: Implications for paleolake basins on Mars. J. Geophys. Res. Planets, 117(E7). doi: 10.1029/2012JE004046.

Kraal, E.R., Asphaug, E., Moore, J.M., Lorenz, R.D., 2006. Quantitative geomorphic modeling of Martian bedrock shorelines. J. Geophys. Res. Planets, 111. E03001. doi: 10.1029/2005JE002567.

Kleinhans, M.G., 2005. Flow discharge and sediment transport models for estimating a minimum timescale of hydrological activity and channel and delta formation on Mars. J. Geophys. Res. Planets, 110(E12). doi: 10.1029/2005JE002521.

Kneissl, T., van Gasselt, S., Neukum, G., 2011. Map-projection-independent crater size-frequency determination in GIS environments—New software tool for ArcGIS. Planet. Space Sci., 59(11), 1243-1254. doi: 10.1016/j.pss.2010.03.015.

Kraal, E.R., Van Dijk, M., Postma, G., Kleinhans, M.G., 2008. Martian stepped-delta formation by rapid water release. Nature, 451(7181), 973. doi: 10.1038/nature06615.

Lemons, D.R., Chan, M.A., 1999. Facies architecture and sequence stratigraphy of fine-grained lacustrine deltas along the eastern margin of late Pleistocene Lake Bonneville, northern Utah and southern Idaho. AAPG bulletin, 83(4), 635-665.

Malin, M.C., Carr, M.H., 1999. Groundwater formation of Martian valleys. Nature, 397(6720), 589. doi: 10.1038/17551.

Malin, M.C., Edgett, K.S., 2000. Evidence for recent groundwater seepage and surface runoff on Mars. Science, 288(5475), 2330-2335. doi: 10.1126/science.288.5475.2330.

Malin, M.C., Bell, J.F., Cantor, B.A., Caplinger, M.A., Calvin, W.M., Clancy, R.T. Lee, S.W., 2007. Context camera investigation on board the Mars Reconnaissance Orbiter. J. Geophys. Res. Planets, 112(E5), E05S04. doi: 10.1029/2006JE002808.

Manent, L.S., El-Baz, F., 1986. Comparison of knobs on Mars to isolated hills in eolian, fluvial and glacial environments. Earth Moon Planets, 34(2), 149-167. doi: 10.1007/BF00055132.

Martín-González, F., de Pablo, M.A., Pacifici, A., 2007. Alignments mapping and structural analysis of western sector of Nepenthes Mensae, Mars. Geophysical Research Abstracts, 9. 07796.

McEwen, A.S., Eliason, E.M., Bergstrom, J.W., Bridges, N.T., Hansen, C.J., Delamere, W.A., Grant, J.A., Gulick, V.C., Herkenhoff, K.E., Keszthelyi, L., Kirk, R.L., Mellon,

M.T., Squyres, S.W., Thomas, N, Weitz, C.M., 2007. Mars reconnaissance orbiter's high resolution imaging science experiment (HiRISE). J. Geophys. Res. Planets, 112(E5), E05S02. doi: 10.1029/2005JE002605.

Michael, G.G., 2013. Planetary surface dating from crater size–frequency distribution measurements: multiple resurfacing episodes and differential isochron fitting. Icarus 226 (1), 885–890. doi: 10.1016/j.icarus.2013.07.004.

Michael, G.G., Neukum, G., 2010. Planetary surface dating from crater size–frequency distribution measurements: Partial resurfacing events and statistical age uncertainty. Earth Planet. Sci. Lett, 294(3), 223-229. doi: 10.1016/j.epsl.2009.12.041.

Michael, G.G., Platz, T., Kneissl, T., Schmedemann, N., 2012. Planetary surface dating from crater size–frequency distribution measurements: spatial randomness and clustering. Icarus 218 (1), 169–177. doi: 10.1016/j.icarus.2011.11.033.

Mikhailova, M.V., 2015. Morphometry of river deltas. Water Resour, 42(1), 52-62. doi: 10.1134/S009780781501008X.

Morrison, R. B.. 1964. Lake Lahontan: geology of southern Carson desert, Nevada (Vol. 401). US Government Printing Office. Retrieved from https://pubs.usgs.gov/pp/0401/report.pdf

Morgan, F., Seelos, F.P., Murchie, S.L., the CRISM Team, 2014, CRISM Analysis Toolkit (CAT), in Gaddis , R.G., Hare, T., and Beyer, R., eds., Summary and Abstracts of the Planetary Data Workshop, June 2012: Open-File Report 2014-1056, U.S. Geological Survey, Reston, VA, USA, p. 125–126.

Murchie, S, et al., 2007. Compact reconnaissance imaging spectrometer for Mars (CRISM) on Mars reconnaissance orbiter (MRO). J. Geophys. Res. Planets, 112(E5). doi: 10.1029/2006JE002682.

Neukum G., Ivanov B.A., Hartmann W.K., 2001. Cratering Records in the Inner Solar System in Relation to the Lunar Reference System. In: Kallenbach R., Geiss J., Hartmann W.K. (eds) Chronology and Evolution of Mars. Space Sciences Series of ISSI, vol 12. Springer, Dordrecht. doi: 10.1007/978-94-017-1035-0_3.

Neukum, G., Jaumann, R., the HRSC Co-Investigator and Experiment Team, 2004. HRSC: the High Resolution Stereo Camera of Mars Express. In: Wilson A. (ed.) Mars Express: The Scientific Payload. ESA, Noordwijk, The Netherlands, SP-1240, 17-35.

Nordstrom, K. F., Jackson, N. L., 2012. Physical processes and landforms on beaches in short fetch environments in estuaries, small lakes and reservoirs: a review. Earth-Science Reviews, 111(1-2), 232-247. doi: 10.1016/j.earscirev.2011.12.004

Oviatt, C.G., 2015. Chronology of Lake Bonneville, 30,000 to 10,000 yr BP. Quaternary Sci. Rev., 110, 166-171. doi: 10.1016/j.quascirev.2014.12.016.

Parker, T.J., Saunders, R.S., Schneeberger, D.M., 1989. Transitional morphology in west Deuteronilus Mensae, Mars: Implications for modification of the lowland/upland boundary. Icarus, 82(1), 111-145. doi: 10.1016/0019-1035(89)90027-4.

Parker, T.J., Gorsline, D.S., Saunders, R.S., Pieri, D.C., Schneeberger, D.M., 1993. Coastal geomorphology of the Martian northern plains. J. Geophys. Res. Planets, 98(E6), 11061-11078. doi: 10.1029/93JE00618.

Parker, T.J., Currey, D.R., 2001. Extraterrestrial coastal geomorphology. Geomorphology, 37(3-4), 303-328. doi: 10.1016/S0169-555X(00)00089-1.

Parker, T.J., Grant, J.A., Franklin, B.J., 2010. The northern plains: A Martian oceanic basin. Lakes on Mars, 249-273. doi: 10.1016/B978-0-444-52854-4.00009-X. Penland, S., Kulp, M.A., 2005. Deltas. In: Schwartz, M. (Ed.), Encyclopedia of Coastal Science. Springer, pp. 362–386.

Perron, J.T., Mitrovica, J.X., Manga, M., Matsuyama, I., Richards, M.A., 2007. Evidence for an ancient martian ocean in the topography of deformed shorelines. Nature, 447(7146), 840. doi: 10.1038/nature05873.

Pondrelli, M., Rossi, A.P., Marinangeli, L., Hauber, E., Gwinner, K., Baliva, A., Di Lorenzo, S., 2008. Evolution and depositional environments of the Eberswalde fan delta, Mars. Icarus, 197(2), 429-451. doi: 10.1016/j.icarus.2008.05.018.

Poulet, F., Bibring, J.P., Mustard, J.F., Gendrin, A., Mangold, N., Langevin, Y., Arvidson, R. E., Gondet, B., Gomez, C., the Omega Team, 2005. Phyllosilicates on Mars and implications for early Martian climate. Nature, 438(7068), 623-627. doi: 10.1038/nature04274.

Rivera- Hernández, F., Palucis, M.C., 2019. Do deltas along the crustal dichotomy boundary of Mars in the Gale crater region record a northern ocean? Geophys. Res. Lett., 46, 8689–8699. doi: 10.1029/2019GL083046.

Schon, S.C., Head, J.W., Fassett, C.I., 2012. An overfilled lacustrine system and progradational delta in Jezero crater, Mars: Implications for Noachian climate. Planet. Space Sci., 67(1), 28-45. doi: 10.1016/j.pss.2012.02.003.

Sunamura, T., 1992. Shore platforms. In: Geomorphology of rocky coasts (Vol. 302) (139-183 pp.) Chichester: Wiley.

Tanaka, K.L., Skinner, J.A., Jr., Dohm, J.M., Irwin, R.P., III, Kolb, E.J., Fortezzo, C.M., Platz, T., Michael, G.G., Hare, T.M., 2014, Geologic map of Mars: U.S. Geological Survey Scientific Investigations Map 3292, scale 1:20,000,000, pamphlet 43 p. doi: 10.3133/sim3292.

Trenhaile, A.S., 1987. Shore platforms. In: The geomorphology of rock coasts (192-239 pp.). Oxford University Press, USA.

Valenciano, A., de Pablo, M.Á., Pacifici, A., 2009. The role of water on the evolution of the Nepenthes Mensae region of Mars. In: Lunar and Planetary Science Conference Abstracts, vol. 40, p#1052.

Vaquero, A.V., Hernández, M.Á. D. P., 2010. La importancia del agua en el modelado de la región de Nepenthes Mensae, Marte. Tecnología y desarrollo, 8, 30. Retrieved from https://revistas.uax.es/index.php/tec_des/article/view/563.

Viviano- Beck, C.E., et al., 2014. Revised CRISM spectral parameters and summary products based on the currently detected mineral diversity on Mars. J. Geophys. Res. Planets, 119(6), 1403-1431. doi: 10.1002/2014JE004627.

Viviano-Beck, C.E., et al., 2015. MRO CRISM Type Spectra Library, NASA Planetary Data System. Retrieved from http://crismtypespectra.rsl.wustl.edu.

Warner, N.H., Gupta, S., Calef, F., Grindrod, P., Boll, N., Goddard, K., 2015. Minimum effective area for high resolution crater counting of martian terrains. Icarus, 245, 198-240. doi: 10.1016/j.icarus.2014.09.024.

Webb, V.E., 2004. Putative shorelines in northern Arabia Terra, Mars. J. Geophys. Res. Planets, 109(E9). doi: 10.1029/2003JE002205.

Wood, L.J., 2006. Quantitative geomorphology of the Mars Eberswalde delta. Geol. Soc. Am. Bull., 118(5-6), 557-566. doi: 10.1130/B25822.1.

Zazo, C., Goy, J.L., Dabrio, C.J., Lario, J., González-Delgado, J.A., Bardají, T., Hillaire-Marcel, C., Cabero, A., Ghaleb, B., Borja, F., Silva, P.G., Roquero, E., Soler, V., 2013. Retracing the Quaternary history of sea-level changes in the Spanish Mediterranean–Atlantic coasts: Geomorphological and sedimentological approach. Geomorphology, 196, 36-49. doi: 10.1016/j.geomorph.2012.10.020.

Zimbelman, J.R., Williams, S.H., Johnston, A.K., Head, J.W., 2004. Lake shorelines: earth analogs for hypothesized Martian coastal features. In: Lunar and Planetary Science Conference Abstracts, vol. 35, p#1683.

Zimbelman, J.R., Williams, S.H., Irwin, R.P., Rivera, J.E., Graves, L., Ghatan, G., 2005 Shorelines in the western United States as analogs for hypothesized shoreline features on MarsF. In: Lunar and Planetary Science Conference Abstracts, vol. 36, p#1733.

Declaration of interests

☒ The authors declare that they have no known competing financial interests or personal relationships that could have appeared to influence the work reported in this paper.

☐The authors declare the following financial interests/personal relationships which may be considered as potential competing interests: